VI.　研究成果の刊行物・別刷

Immunity

The Ly49Q Receptor Plays a Crucial Role in Neutrophil Polarization and Migration by Regulating Raft Trafficking

Shigemi Sasawatari,[1] Mariko Yoshizaki,[1] Choji Taya,[2] Aya Tazawa,[1] Kaori Furuyama-Tanaka,[1] Hiromichi Yonekawa,[2] Taeko Dohi,[1] Andrew P. Makrigiannis,[3] Takehiko Sasazuki,[4] Kayo Inaba,[5] and Noriko Toyama-Sorimachi[1,*]

[1]Department of Gastroenterology, Research Institute, International Medical Center of Japan, Toyama1-21-1, Shinjuku-ku, Tokyo 162-8655, Japan

[2]Department of Laboratory Animal Science, The Tokyo Metropolitan Institute of Medical Science, 2-1-6 Kami-kitazawa, Setagaya-ku, Tokyo 156-8506, Japan

[3]Department of Biochemistry, Microbiology and Immunology, University of Ottawa, Faculty of Medicine, 451 Smyth Road, Roger Guindon Hall, Rm 4226, Ottawa, ON K1H 8M5, Canada

[4]International Medical Center of Japan, Toyama1-21-1, Shinjuku-ku, Tokyo 162-8655, Japan

[5]Department of Animal Development and Physiology, Graduate School of Biostudies, Kyoto University, Kitashirakawa-Oiwake-cho, Sakyo-ku, Kyoto 606-8502, Japan

*Correspondence: nsorima@ri.imcj.go.jp

DOI 10.1016/j.immuni.2010.01.012

SUMMARY

Neutrophils rapidly undergo polarization and directional movement to infiltrate the sites of infection and inflammation. Here, we show that an inhibitory MHC I receptor, Ly49Q, was crucial for the swift polarization of and tissue infiltration by neutrophils. During the steady state, Ly49Q inhibited neutrophil adhesion by preventing focal-complex formation, likely by inhibiting Src and PI3 kinases. However, in the presence of inflammatory stimuli, Ly49Q mediated rapid neutrophil polarization and tissue infiltration in an ITIM-domain-dependent manner. These opposite functions appeared to be mediated by distinct use of effector phosphatase SHP-1 and SHP-2. Ly49Q-dependent polarization and migration were affected by Ly49Q regulation of membrane raft functions. We propose that Ly49Q is pivotal in switching neutrophils to their polarized morphology and rapid migration upon inflammation, through its spatiotemporal regulation of membrane rafts and raft-associated signaling molecules.

INTRODUCTION

The rapid infiltration of affected tissues by neutrophils is critical for the host defense against invading bacteria and response to acute inflammation, and neutrophils have specific inherent properties for polarization and migration. They migrate to sites of infection and inflammation along a gradient of chemoattractants, such as chemokines, and the bacterially derived tripeptide fMet-Leu-Phe (fMLP). Neutrophils respond to the shallow chemoattractant gradient by becoming morphologically polar, with a lamellar pseudopod at the cell's leading edge (lamellipodia) and a rounded contractible trailing edge (uropodia) (Affolter and Weijer, 2005; Downey, 1994; Servant et al., 2000). Interestingly, exposure to a single concentration of chemoattractant (i.e., without a gradient), can trigger neutrophil polarization (Wong et al., 2006; Xu et al., 2003), and the neutrophil's pseudopod is far more responsive to chemoattractants than are its sides and uropod (Xu et al., 2003; Zigmond et al., 1981).

Studies aimed at understanding the molecular mechanisms of these neutrophilic attributes have demonstrated specific roles for cellular signals and cytoskeletal assemblies that restrict "frontness" and "backness" in a neutrophilic cell line derived from HL-60 (Wong et al., 2006; Xu et al., 2003). The main feature of frontness is the protruding pseudopod, which contains polymerized F-actin and is dependent on a heterotrimeric G protein (Gi), PIP3, the Rho GTPase Rac, and F-actin. In contrast, "backness" is characterized by a contractile actomyosin system, and its formation is induced by signals that include a different heterotrimeric G protein (Gα12 and Gα13), RhoA, a Rho-dependent kinase, ROCK, and myosin II. Backness signals inhibit frontness signals and vice versa. Localized incompatible actin responses triggered by different G proteins, actin polymerization in the front and actomyosin contraction at the back, provide a partial explanation of how polarity is organized in neutrophils. However, these signaling molecules are widely expressed in various cell types, and their spatiotemporal regulation is still largely unknown. Therefore, the molecular basis for the specific behaviors of polarized neutrophils is still not fully explained by the information on the roles and locations of these signaling molecules.

Inhibitory receptors possessing one or more immunoreceptor tyrosine-based inhibitory motifs (ITIMs) play crucial roles in the regulation of a wide range of immune responses (Lanier, 1998). Ly49Q is an ITIM-bearing inhibitory receptor belonging to the Ly49 family (Makrigiannis et al., 2002; Toyama-Sorimachi et al., 2004). Inhibitory NK receptor family members recognize MHC class I or its related molecules to distinguish target cells from nontarget ones (Lanier, 1998). Recognition of the self MHC class I molecules on the target cell induces a signal via ITIM-bearing inhibitory receptors that inhibits NK cell cytotoxic functions and cytokine production (Lanier, 1998). Like other NK receptor

family members, Ly49Q recognizes classical MHC class I molecules such as H-2K^b (Scarpellino et al., 2007; Tai et al., 2007). The ITIM of Ly49Q can recruit phosphatases SHP-1 and SHP-2 in a tyrosine-phosphorylation-dependent manner (Toyama-Sorimachi et al., 2004). However, even though its high sequence similarity and chromosomal location have led to Ly49Q being classified as an NK receptor family member, it is not expressed on either NK cells or T cell subsets. Rather, it is preferentially expressed on Gr-1$^+$ cells, including monocytes and macrophages, plasmacytoid dendritic cells (pDCs), and neutrophils (Omatsu et al., 2005; Tai et al., 2008; Toyama-Sorimachi et al., 2004).

Recently, in a report on Ly49Q-deficient mice, we showed that Ly49Q is important for pDC function, including the TLR9-triggered production of type I IFN and IL-12 (Tai et al., 2008). We also showed that the impaired cytokine production in Ly49Q-deficient cells was due to dysregulation of both the trafficking of TLR9 and CpG-containing endolysosomes and the TLR9-mediated activation of MAP kinase (Yoshizaki et al., 2009). Using immunohistochemistry, we also found that Ly49Q colocalizes not only with TLR9 and CpG, but also with Rab5 and phosphorylated MAP kinases in endosomes. Thus, Ly49Q appears to be involved in membrane dynamics, especially in the spatiotemporal regulation of endosome-lysosome trafficking and the associated signaling.

We also reported that Ly49Q is involved in the rapid induction of macrophage spreading and polarization, with marked formation of lamellipodia and filopodia (Toyama-Sorimachi et al., 2004). Several studies have shown that membrane trafficking is crucial for polarization and migration in various cell types (Mañes et al., 1999; Pierini et al., 2003; Polishchuk et al., 2004). These and our earlier observations, including on Ly49Q-mediated endosome-lysosome trafficking, led us to hypothesize that Ly49Q contributes to the organization of cell polarity and the subsequent migration of inflammatory cells by regulating membrane trafficking. Indeed, Ly49Q is itself internalized in a raft-dependent manner, and its internalization and trafficking are regulated by its ITIM and by the activity of associated phosphatases (Yoshizaki et al., 2009). Here, we demonstrate that Ly49Q was essential for the organization of neutrophil polarity and their subsequent invasion of extravascular tissues during early inflammation. Importantly, in the absence of inflammatory stimuli, Ly49Q inhibited the firm adhesion and spreading of neutrophils by suppressing the formation of focal adhesion complexes, indicating that Ly49Q helps prevent the deleterious adhesion of neutrophils during the steady state. Interestingly, Ly49Q associated with the inhibitory phosphatase SHP-1 in the steady state, but it recruited SHP-2, which plays a largely positive role in cell activation, adhesion, and migration, in the presence of inflammatory stimuli. Therefore, these apparently opposite functions of Ly49Q in the steady state and the inflammatory state appeared to be mediated by recruiting an additional associated effector phosphatase. We propose a mechanism in which Ly49Q directs the organization of neutrophil polarization, as well as their migration to sites of inflammation, by regulating membrane raft functions. These membrane raft functions permit the rapid reorganization of neutrophils in the presence of inflammatory signals, and maintain neutrophil homeostasis in the absence of such signals.

RESULTS

Expression and Distribution of Ly49Q on Neutrophils

We previously reported that Ly49Q is expressed on Gr-1$^+$ cells, including monocytes, macrophages, and pDCs, in the mouse spleen, bone marrow (BM), and fetal liver (Omatsu et al., 2005; Toyama-Sorimachi et al., 2004). We first confirmed that neutrophils in mouse peripheral blood and BM expressed Ly49Q under steady-state conditions (Figure S1A available online). Infiltrating neutrophils that had migrated to the peritoneal cavity in response to casein or to the air pouches in response to zymosan also expressed Ly49Q, showing the typical lobulated nucleus (Figure 1A, see also Figure S1A). Ly49Q colocalized with H-2K^b not only at the cell surface, but also in endosomal vesicles, suggesting that Ly49Q was internalized together with H-2K^b (Figure 1B, see also Figure S1B). This was consistent with our recent observation in pDCs that Ly49Q is internalized and localizes to endosomes (Yoshizaki et al., 2009). Because the association of Ly49Q with H-2K^b is stable under acidic conditions (Yoshizaki et al., 2009), it is likely that the Ly49Q-H-2K^b interaction is sustained in the internalized vesicles.

To investigate whether Ly49Q contributes to the polarization of neutrophils in response to inflammatory signals, neutrophils obtained from Ly49Q-deficient or control littermate mice were stimulated with fMLP, and their adoption of the polarized phenotype and chemotactic migration were examined. The control Ly49Q$^{+/}$ neutrophils responded to fMLP by spreading their cytoplasm and adopting the polarized distribution of polymerized actin and of CD44, a known uropodial marker (Figures 1C and 1D) (del Pozo et al., 1995). In contrast, in Ly49Q-deficient (*Klra17* $^{/}$) neutrophils, the distribution of the polymerized actin and of CD44 remained uniform in the presence of fMLP (Figures 1C and 1D). The percentage of polarized cells among the fMLP-treated *Klra17*$^{-/-}$ neutrophils was significantly ($p < 0.0002$) lower than among the *Klra17*$^{+/-}$ neutrophils (Figure 1E). Consistent with this, significantly ($p < 0.05$) fewer *Klra17*$^{-/-}$ neutrophils showed fMLP-induced chemotactic migration than *Klra17*$^{+/-}$ neutrophils (Figure 1F). *Klra17*$^{-/-}$ neutrophils also showed reduced chemotaxis to KC compared with *Klra17*$^{+/-}$ neutrophils (Figure 1F), whereas no difference in ROS production in response to fMLP was observed between the *Klra17*$^{-/}$ and *Klra17*$^{+/-}$ neutrophils (Figure S1C). Furthermore, in vivo, the number of neutrophils infiltrating the air pouch 3 hr after zymosan or *E. coli* inoculation and the neutrophilic migration to inflamed tissue were reduced in the Ly49Q-deficient mice (Figures 1G and 1H). To confirm the role of MHC class I as a Ly49Q ligand in neutrophil migration, we examined the chemotactic activity of *B2m*$^{-/-}$ neutrophils in vitro. The migration of *B2m*$^{-/-}$ neutrophils to the chemoattractants was significantly ($p < 0.001$) reduced (Figure 1I), suggesting that the Ly49Q-MHC class I interaction plays an important role in neutrophil migration. Taken together, these results indicated that Ly49Q plays an important role in the polarity formation and migration of neutrophils.

Constitutive Association of SHP-1 and Activation-Dependent Recruitment of SHP-2 to Ly49Q

To understand how Ly49Q is involved in neutrophil polarization, we compared the intracellular distribution of Ly49Q-related molecules in neutrophils from Ly49Q-deficient mice and their

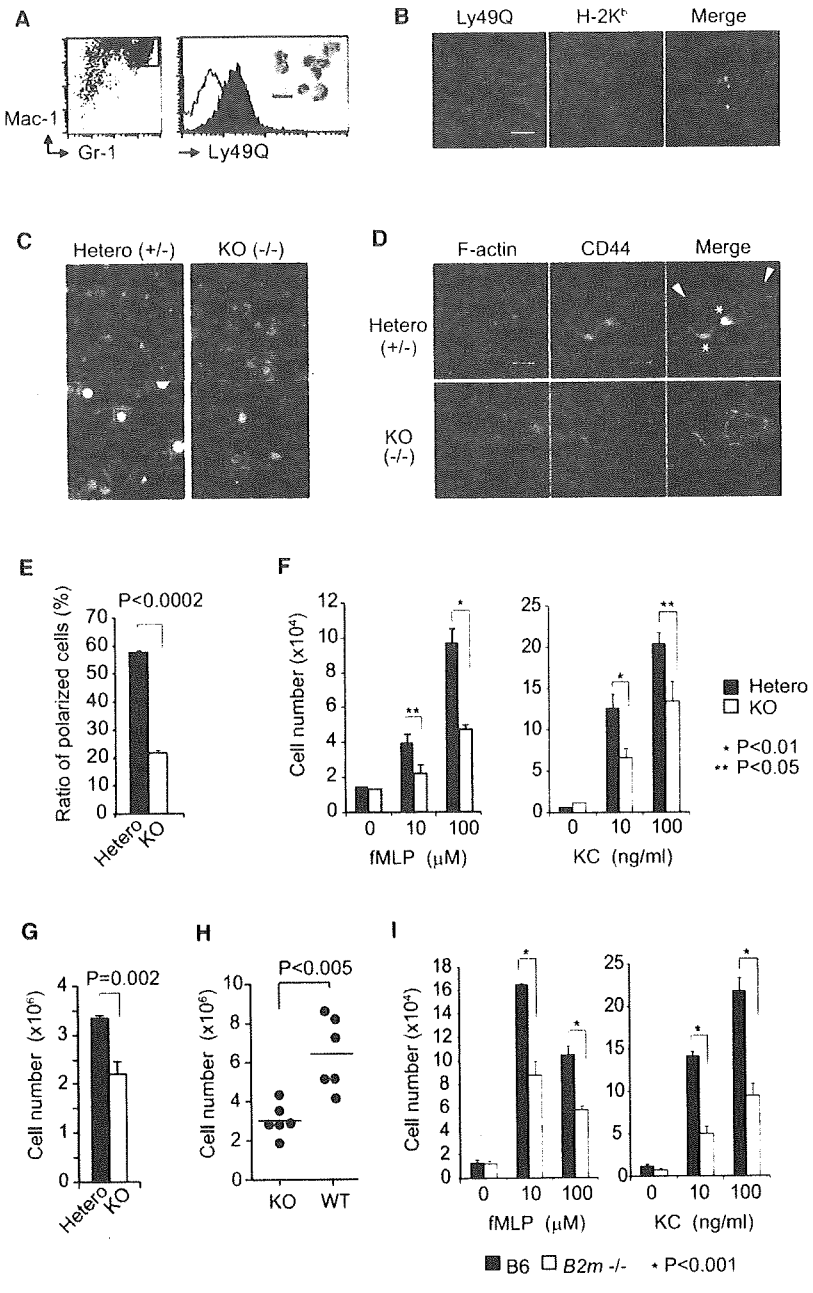

Figure 1. Impaired Polarization and Migration of Neutrophils from Ly49Q-Deficient Mice

(A) Expression of Ly49Q on neutrophils from inflamed dorsal air pouch of C57BL/6 mice. Cells prepared from inflamed dorsal air pouch were stained with FITC-conjugated anti-Gr-1 and PE-conjugated anti-Mac-1 (CD11b) with a biotin-conjugated anti-Ly49Q (NS34, filled histograms) or biotin-conjugated isotype-matched (rat IgG2a, open histograms) antibody, followed by streptavidin-conjugated APC. Cells expressing both Gr-1 and Mac-1 were analyzed for the expression of Ly49Q. Scale bars (insets), 20 μm.

(B) Colocalization of Ly49Q and H-2K^b in neutrophils. Confocal images show casein-induced neutrophils stained with anti-Ly49Q and anti-H-2K^b. Scale bars, 5 μm.

(C) Phase-contrast microscopic analysis of neutrophil polarization. Neutrophils were enriched from the BM of Ly49Q-deficient (KO) or control littermate (hetero) mice by removing B220$^+$ cells by magnetic cell sorting and were treated with fMLP (25 μM). The adhered cells were fixed with 4% formalin and microscopically analyzed. The lower photographs show a higher magnification.

(D) Impairment of fMLP-induced polarization in Ly49Q-deficient neutrophils (KO). Neutrophils were prepared as described in (C). Confocal images show the cytoskeletal organization (F-actin) stained with Alexa594-labeled phalloidin (red) and uropodia stained with FITC-labeled anti-CD44 (green) in fMLP-treated neutrophils. Arrowheads and asterisks indicate lamellipodia and uropodia, respectively. No obviously polarized distribution of F-actin or CD44 was observed in the Ly49Q KO neutrophils.

(E) Quantitative analysis of polarized neutrophils in response to fMLP. Neutrophils prepared as described in (D) were photographed, and the cells showing a polarized actin structure and CD44 localization at the uropodia were counted. Over 600 cells within three independent fields were counted. Data are presented as mean ± SEM.

(F) Impairment of the chemotactic migration of Ly49Q-deficient neutrophils. The BM neutrophils that had migrated in response to fMLP or KC to the lower wells of chemotaxis chambers were counted. The results from three independent experiments are shown. Data are presented as mean ± SEM.

(G and H) Neutrophil migration into an air pouch. The neutrophil migration in vivo was examined using the dorsal air pouch model. Three hours after zymosan injection (0.5 mg/mouse) (G) or *E. coli* (DH5 strain, 3 × 10^8 cfu/mouse) (H) into the air pouch, the neutrophils were collected from the air pouch and counted. More than four mice from each group were examined. Data are presented as mean ± SEM.

(I) Impairment of the chemotactic migration of β2m-deficient neutrophils. The BM neutrophils that migrated in response to fMLP or KC to the lower wells of chemotaxis chambers were counted. The results from three independent experiments are shown. Data are presented as mean ± SEM.

control littermates. In the absence of fMLP, H-2K^b (the Ly49Q ligand) was predominantly localized to the plasma membrane in *Klra17*$^{+/-}$ neutrophils (Figure 2A). Distribution of H-2K^b appeared to form clusters. Notably, SHP-1 was colocalized with H-2K^b in the absence of fMLP in the *Klra17*$^{+/-}$ neutrophils (Figure 2A), and this colocalization was Ly49Q dependent because it was not observed in the *Klra17*$^{-/-}$ neutrophils (Figure 2A). We confirmed the association between SHP-1 and H-2K^b in the absence of fMLP by immunoprecipitation (Figure S3). Interestingly, in fMLP-treated *Klra17*$^{+/-}$ neutrophils, H-2K^b and SHP-1 together relocated from the cell surface to endosomal compartments, with many positive immunofluorescent

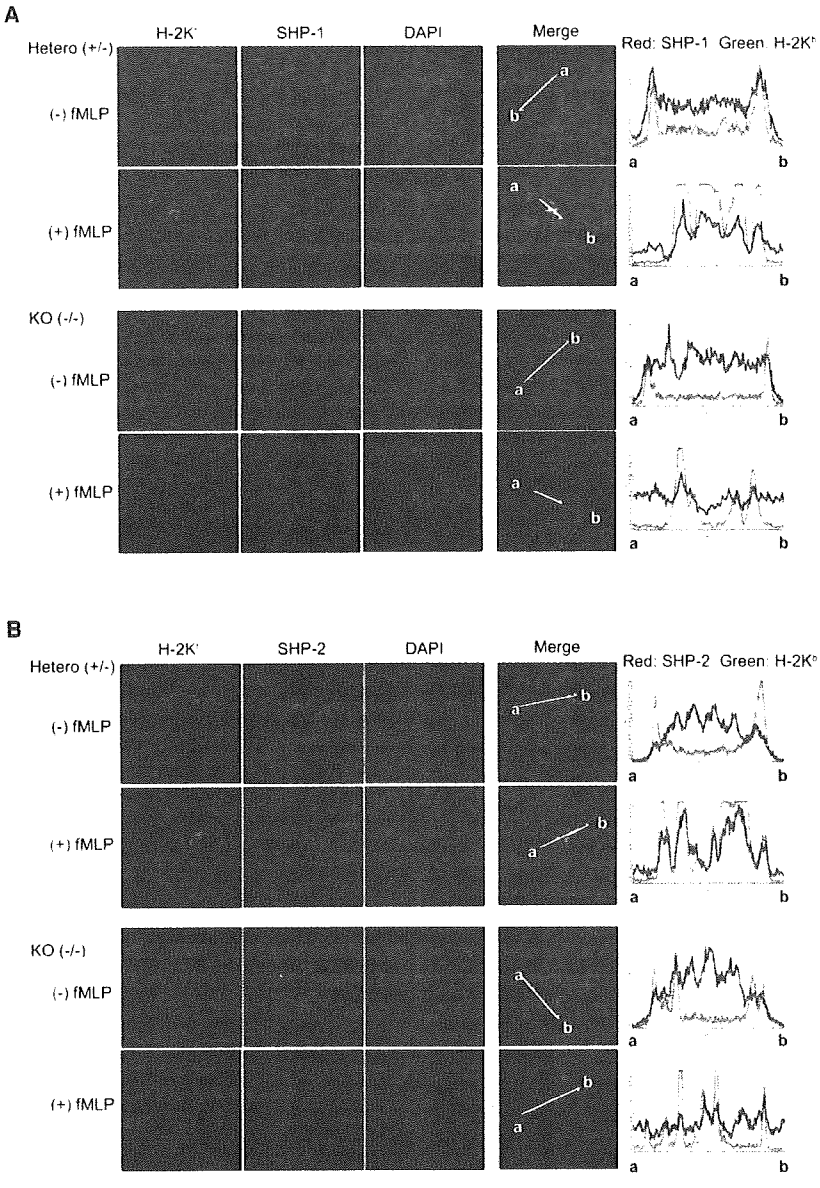

Figure 2. Intracellular Distribution of Ly49Q-Related Molecules in Neutrophils

The colocalization of H-2K^b with SHP-1 (A) or with SHP-2 (B) in the absence or presence of fMLP was examined by confocal microscopy. Neutrophils were enriched from the BM of *Klra17*$^{-/-}$ or littermate *Klra17*$^{+/}$ mice by removing the B220$^+$ cells, treated with fMLP (25 μM) at 37°C for 40 min, and subsequently stained with anti-H-2K^b (green) in combination with anti-SHP-1 or anti-SHP-2 (red). The nuclei were visualized using DAPI. Histograms at the right show the profiles of H-2K^b (green) and the SHPs (red) along the white arrows. All data are representative of three independent experiments.

signals in the perinuclear region. In contrast, even in the presence of fMLP, the *Klra17*$^{-/-}$ neutrophils showed neither SHP-1 colocalization with H-2K^b nor the efficient translocation of H-2K^b to the endosomal compartments, although the amount of H-2K^b in the *Klra17*$^{-/-}$ neutrophils appeared to be reduced. This result might have been due to the structural instability of H-2K^b in the absence of Ly49Q during endosomal acidification. These results indicated that SHP-1 was constitutively associated with Ly49Q, which interacted with H-2K^b in *cis* at the cell surface in the steady state, and that the Ly49Q-H-2K^b-SHP-1 complexes were internalized and transported to the perinuclear endosomal compartments in response to fMLP stimulation.

In contrast to SHP-1, SHP-2 was not colocalized with H-2K^b in the steady state (Figure 2B). Notably, fMLP stimulation induced the colocalization of SHP-2 with H-2K^b and the redistribution of SHP-2 to the perinuclear endosomal compartments. Importantly, the recruitment and transport of SHP-2 was Ly49Q dependent, as it was not observed in *Klra17*$^{-/-}$ neutrophils. These results indicate that Ly49Q is responsible for the fMLP-dependent recruitment of SHP-2 to membrane compartments from the cytoplasm. In addition, Ly49Q, along with the SHPs and H-2K^b, was localized to lipid rafts, as visualized by cholera toxin B subunit (CTB) binding, at the cell surface and in the endosomal compartments (Figure 3A). These results indicate that Ly49Q is responsible for recruiting SHP-2 to membrane rafts and for the trafficking of the rafts and the associated SHP-1 and SHP-2. A previous study established that SHP-2 partitioning to raft compartments triggers Rho activation and subsequently integrin-mediated signaling (Lacalle et al., 2002). Therefore, the Ly49Q-dependent recruitment of SHP-2 to rafts during neutrophil polarization indicates that Ly49Q has an important role in the regulation of polarity formation. These data also demonstrate that Ly49Q differentially associates with SHP phosphatases and regulates neutrophil functions in a different manner, depending on the presence or absence of the fMLP stimulus.

Ly49Q-Dependent Internalization and Movement of Lipid Rafts

Previous studies reported that the trafficking and redistribution of lipid rafts are critical for cell polarization and directional migration (Mañes et al., 1999; Pierini et al., 2003; Polishchuk et al., 2004). Therefore, we hypothesized that Ly49Q regulates the trafficking of endocytosed rafts in neutrophils to induce polarity. To test this hypothesis, raft distribution was compared between *Klra17*$^{+/-}$ and *Klra17*$^{-/-}$ neutrophils. In the presence of fMLP, polarized *Klra17*$^{+/-}$ neutrophils efficiently internalized raft components (Figure 3B). The internalized rafts gathered at the perinuclear region, similar to the distribution of H-2K^b shown in

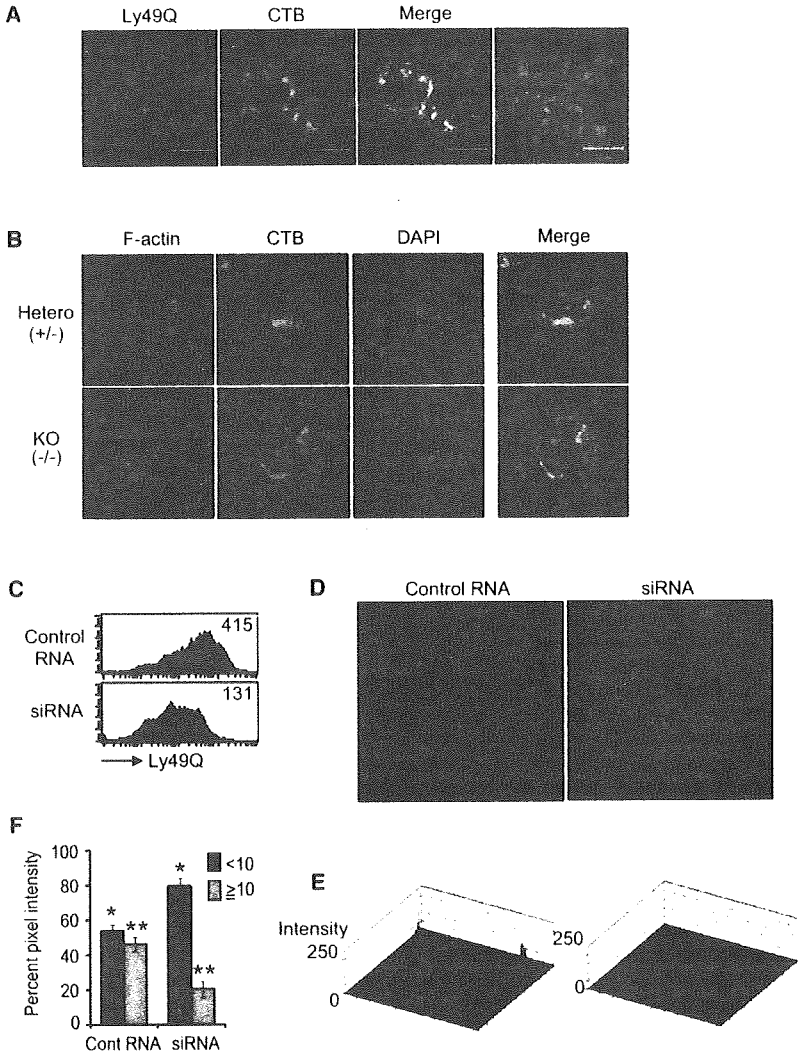

Figure 3. Ly49Q-Dependent Raft Endocytosis

(A) Colocalization of Ly49Q with lipid rafts. RAW264 cells were transfected with FLAG-tagged Ly49Q and stained for Ly49Q with anti-FLAG (red) and for rafts with CTB (green). Confocal images from a single plane are shown.

(B) Lipid raft internalization and redistribution during fMLP-induced neutrophil polarization. Neutrophils enriched from BM were incubated at 37°C for 40 min in the presence of fMLP and stained for rafts with CTB (green) and for F-actin with phalloidin (red). Nuclei were visualized with DAPI. These data are representative of three or four independent experiments.

(C) Decreased expression of Ly49Q in X63 cells after introducing Ly49Q-specific siRNA. The X63 myeloma cell line, which expresses Ly49Q endogenously, was transfected with Ly49Q-specific siRNA or control RNA and then analyzed for Ly49Q expression by flow cytometry. Histograms show the mean fluorescence intensities.

(D) Confocal images of lipid rafts in the Ly49Q gene-targeted X63 myeloma cells. After 72 hr of siRNA transfection, the cells were stained with CTB to visualize the lipid rafts and analyzed by confocal microscopy. This figure is representative of two independent experiments.

(E and F) Quantitative analyses of the intracellular raft distribution in Ly49Q gene-targeted X63 myeloma cells. The CTB fluorescence intensity in the confocal images shown in (D) is represented by 3D histograms (E) according to the LC500 analysis program. Each 3D histogram represents about 15–20 cells, and each peak indicates the fluorescence intensity of one cell. Bar graph (F) shows the percentage of pixels with a signal intensity less than 10 (dark gray bars) or greater than 10 (light gray bars). The fluorescence signal intensities of ten non-overlap photographs for each condition were digitalized for the pixel analyses. *$p < 0.0002$; **$p < 0.0002$. Data are presented as mean ± SEM.

Figure 2. In contrast, in the *Klra17*$^{-/-}$ neutrophils, the rafts largely remained at or near the cell surface, and the efficient redistribution of raft components was not observed in the presence of fMLP. In the absence of fMLP, there was little difference in the distribution of the rafts between *Klra17*$^{+/-}$ and *Klra17*$^{-/-}$ neutrophils, and the staining was mainly observed at the cell surface (data not shown).

To confirm the importance of Ly49Q in raft behavior, we carried out siRNA gene-targeting experiments using X63 myeloma cells expressing endogenous Ly49Q. The intracellular distribution of raft components, labeled by CTB binding, decreased in the Ly49Q-specfic siRNA-expressing X63 cells, but not in cells expressing a control RNA (Figures 3C and 3D). Quantitative analysis of the CTB fluorescence and a comparison of the areas covered by intracellular CTB-labeled rafts, by counting the corresponding pixels, also indicated that the decreased Ly49Q expression reduced intracellular raft components (Figures 3E and 3F). A similar impairment in raft distribution was observed in Ly49Q^{lo}, but not in Ly49Q^{hi} RAW264 clones (Yoshizaki et al., 2009) (Figure S2), also supporting an important role for Ly49Q in raft trafficking.

Importance of Ly49Q in the Persistence of Raft-Mediated Signaling

We next investigated whether the dysregulated raft behavior in *Klra17*$^{-/-}$ neutrophils affected fMLP-triggered signals, which are transduced at lipid rafts (Sitrin et al., 2006). Lipid rafts have been shown to serve as an important signaling platform for various receptors, including chemokine receptors (Gómez-Moutón et al., 2004; Mañes et al., 2001; Sitrin et al., 2006). After ligand binding to a chemokine receptor, a heterotrimeric GTPase is activated, which is coupled to downstream signaling pathways by mechanisms such as the activation of Src family kinases (Thelen, 2001). Therefore, we focused on raft-associated and G protein-coupled receptor (GPCR)-proximal kinases and found that the Src kinase activation induced by fMLP was severely

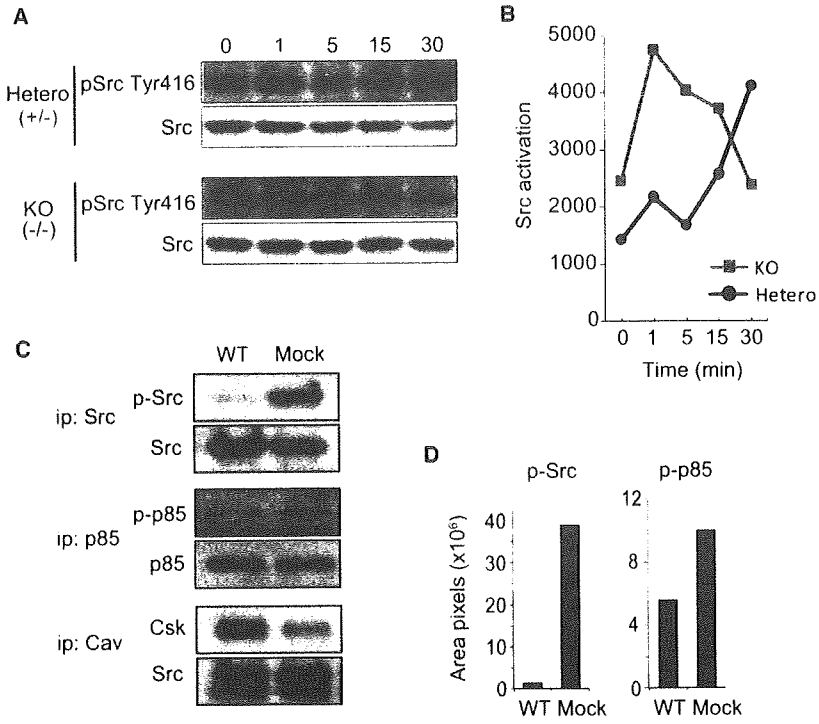

Figure 4. Crucial Role of Ly49Q in the Kinetic Regulation of Src Activity

(A) Activation of Src kinase in neutrophils in the presence of fMLP. Neutrophils enriched from BM were treated with fMLP (25 μM) for the indicated periods (in minutes), and the phosphorylation of Src kinase at Tyr416 was examined by immunoblotting.

(B) Relative amount of Src kinase phosphorylated at Tyr416 in fMLP-treated neutrophils. Bands of the phosphorylated Src and total Src were quantified as described in Experimental Procedures. The y axis values are the amounts of active Src relative to the amount of total Src.

(C and D) Effect of Ly49Q expression on raft-associated signaling molecules. Cell lysates of WEHI3 transfectants were prepared, and immunoprecipitation and immunoblot analyses with the indicated antibodies were performed. The precipitates were analyzed by immunoblotting with the antibodies indicated (C). The signal intensities of the phosphorylated Src and PI3 kinases were digitalized according to the LAS-3000 analysis program and are shown as bar graphs (D). All data are representative of three independent experiments.

impaired in *Klra17*$^{-/-}$ neutrophils. The amount of Src kinases phosphorylated on Tyr416 was substantially increased 1 min after fMLP treatment in the *Klra17*$^{-/-}$ neutrophils (Figures 4A and 4B), but this activation was transient and the amount of phosphorylated Src kinase had drastically decreased by 30 min after the treatment. In contrast, in the *Klra17*$^{+/}$ neutrophils, there was an early, moderate activation of Src kinase, with the amount of active Src kinase increasing at each time point. During fMLP treatment, the total amount of Src kinase gradually decreased in the *Klra17*$^{+/-}$ neutrophils, but not in the *Klra17*$^{-/-}$ neutrophils, consistent with the accepted understanding that active Src is proteolytically degraded (Ben-Neriah, 2002). These observations were also consistent with the recruitment of SHP-2 by Ly49Q because SHP-2 positively regulates Src kinase activity (Zhang et al., 2004). Given that Ly49Q recruited SHP-2 to rafts and maintained its association with SHP-2, even after the raft components had been transported to the perinuclear endosomal compartments, Src kinase may be active throughout its association with the rafts, in the presence of Ly49Q.

Interestingly, the amount of Tyr416-phosphorylated Src kinase at 0 min was higher in the *Klra17*$^{-/-}$ neutrophils than in the *Klra17*$^{+/-}$ neutrophils after normalizing the activated Src kinase to the total amount of Src kinase in the preparations (Figure 4B). This may suggest that Ly49Q inhibits Src kinase in the absence of stimuli. To confirm the inhibitory function of Ly49Q, the mouse myeloid cell line WEHI3, which does not express endogenous Ly49Q, was transfected with a Ly49Q expression plasmid, and the effects on Src and related signaling molecules were examined. The WEHI3 cell line was derived from BALB/c mice and expresses H-2^{d}, but not H-2^{b} (Ralph et al., 1976). As recently reported, Ly49Q interacts with H-2D^{d}, so we expected that Ly49Q would interact with its MHC class I ligand in the WEHI3 cells (Scarpellino et al., 2007). The Src kinase in WEHI3 cells transfected with empty vector (mock) was constitutively phosphorylated at Tyr416 in the steady state (Figure 4C). When Ly49Q was expressed in the WEHI3 cells, phosphorylation of Src kinase at Tyr416 was almost completely inhibited (Figure 4C). Notably, the immunoprecipitation of Ly49Q-expressing lysates with antibodies to caveolin-1, an important raft-associated molecule, also brought down C-terminal Src kinase (Csk), showing that the exogenous Ly49Q recruited Csk to the raft compartment (Figure 4C) (Parton and Richards, 2003). Because Csk negatively regulates Src kinase activity (Zhang et al., 2004), inhibition of Src by Ly49Q may be mediated by a Csk-dependent mechanism. In addition to inhibiting the tyrosine phosphorylation of Src kinase, the expression of Ly49Q inhibited the tyrosine phosphorylation of the PI3 kinase p85 (Figures 4C and 4D). Taken together, these results strongly suggest that, on one hand, Ly49Q inhibits Src and PI3 kinase activity in the steady state, but on the other, Ly49Q is necessary for the sustained activation of Src kinase, probably through the recruitment of SHP-2 to the raft compartment in the presence of fMLP. Because Src kinase has an essential role in cell polarization and migration (Charest and Firtel, 2007; Grande-García et al., 2007), our findings strongly suggested that Ly49Q-regulated Src activation contributes to neutrophil polarization and migration.

Inhibition of Neutrophil Infiltration into Inflammatory Sites in Tg Mice Expressing Ly49Q-YF

To clarify the importance of its ITIM sequence in promotion of polarization and migration by Ly49Q, we analyzed transgenic

mice expressing a mutant of Ly49Q lacking an ITIM domain (Ly49Q-YF), which was designed to function as a dominant-negative isoform for ITIM-dependent functions (Toyama-Sorimachi et al., 2004). The ligand-binding ability of Ly49Q-YF was confirmed by both flow cytometry analyses of H-2K^b tetramer binding (Figures S3A and S3B) and coimmunoprecipitation experiments (Figure S3D). Ly49Q-YF formed heterodimers with Ly49Q-WT (Figure S3E). The dominant-negative function of Ly49Q-YF was validated by examining the effects of its expression along with Ly49Q-WT on PI3 kinase and Src family kinases (Figures S3F and S3G). We also found that the phosphorylation of Ly49Q-associated SHP-2, and probably that of SHP-1, was substantially diminished in the presence of Ly49Q-Ly49Q-YF heterodimers, indicating that the dimers required both ITIMs to fully exert their functions (Figure S3H). The dominant-negative function of Ly49Q-YF was further confirmed by its abrogation of the fMLP-induced changes in tyrosine phosphorylation in neutrophils from Ly49Q-YF Tg mice (Figure S3I).

To determine whether the ITIM of Ly49Q is involved in neutrophil migration, we examined the ability of neutrophils to infiltrate inflammatory sites. The infiltration of air pouches by neutrophils was assessed by inoculating them with zymosan and evaluating the amount of infiltration 3 hr later. We found a significant ($p = 0.00001$) decrease in the number of infiltrating neutrophils in the Ly49Q-YF Tg mice (Figure 5A). In contrast, the neutrophilic infiltration into air pouches at the same time point was significantly ($p = 0.03$) greater in the Ly49Q-WT Tg mice than in their control littermates (Figure 5A). By 6 to 18 hr after zymosan injection, the difference in the number of infiltrating neutrophils between the Tg and littermate control mice was no longer significant (data not shown, $p > 0.2$). We further confirmed the impairment of neutrophil migration using Matrigel chambers for in vitro invasion assays. As shown in Figures 5B and 5C, significantly ($p < 0.005$) fewer Ly49Q-YF than Ly49Q-WT neutrophils migrated in vitro (Figure 5C). These results indicated that the ITIM of Ly49Q is important for chemokine-induced neutrophil infiltration into tissues.

Critical Role of the Ly49Q ITIM in Organizing the Cellular Polarity of Neutrophils

To clarify whether the impaired migration of the Ly49Q-YF neutrophils was associated with impaired cellular polarity, we examined of the adoption of polarity by Ly49Q-YF neutrophils. As shown in Figure 5D, in the presence of fMLP, the Ly49Q-WT neutrophils clearly became polarized, with a ruffled lamellipodia, a contracting uropodia, and a nucleus with a well-organized lobulated structure. Neutrophils prepared from control littermates also showed a polarized morphology in response to fMLP. In contrast, the spreading Ly49Q-YF neutrophils did not exhibit clear polarization, and a number of cells showed an unusual folding of the lobulated nucleus (Figure 5D). An examination of filamentous actin confirmed that both actin polymerization and the organization of cell polarity were impaired in the Ly49Q-YF neutrophils (Figures 5E and 5F). In the Ly49Q-YF neutrophils, the raft internalization and subsequent redistribution in response to fMLP was also severely impaired, and most rafts remained at the cell surface (Figure 5G). In contrast, the Ly49Q-WT neutrophils and the non-Tg neutrophils, which expressed endogenous Ly49Q, showed internalization of the raft compartments and their redistribution to the perinuclear region. When the intracellular distribution of Ly49Q itself was examined, most Ly49Q-WT was at the plasma membrane in the absence of fMLP (Figure 5H, see also Figure S3J). After fMLP treatment, Ly49Q-WT was clearly internalized and transported to the perinuclear region, consistent with the redistribution of the H-2K^b and SHP phosphatases shown in Figure 2 (Figure 5H, see also Figure S3J). In contrast, Ly49Q-YF was localized to the perinuclear regions even in the absence of fMLP, and its location did not change with fMLP treatment (Figure 5H, see also Figure S3J). Therefore, the fMLP-triggered raft movements were accompanied by the redistribution of Ly49Q and were dependent on its ITIM. These results indicated that the Ly49Q-dependent raft redistribution was controlled by the ITIM-dependent trafficking machinery of Ly49Q itself.

Inhibition of Neutrophil Adhesion and Spreading by Ly49Q in the Absence of Chemoattractant

We next examined the roles played by Ly49Q in the steady state because the inhibition of the Src and PI3 kinase activities might affect cell behavior. Since both kinases are important for the formation of focal adhesions, we compared the adhesiveness of Ly49Q Tg-derived neutrophils in the absence of chemoattractant stimuli with that of control B6 neutrophils. The quantitative adhesion assay showed no obvious difference in the adhesion of Ly49Q-YF compared with control B6 neutrophils, in the presence or absence of fMLP, although a slight inhibition of adhesion was observed in the Ly49Q-WT neutrophils in the absence of fMLP (Figure 6A). However, microscopic analyses revealed marked morphological differences between the Ly49Q-WT and Ly49Q-YF neutrophils in the absence of fMLP. The Ly49Q-WT neutrophils were bright, round, and easily detached from the substrate by shaking (Figure 6B), whereas the Ly49Q-YF neutrophils spread and adhered more tightly. The Ly49Q-YF neutrophils appeared dark and had a flat, elongated morphology with protrusions. Staining for paxillin, a scaffolding protein essential for the stable formation of focal adhesions (Webb et al., 2004), showed it to be attenuated at the focal adhesion-like structures in the Ly49Q-WT neutrophils, verifying their decreased adhesiveness (Figure 6B). There was no substantial difference in the expression levels of adhesion molecules, such as integrins between Ly49Q-WT and Ly49Q-YF neutrophils (data not shown).

We further confirmed this inhibitory effect using WEHI3 transfectants expressing Ly49Q-WT, Ly49Q-YF, or empty plasmid (Figure 6C). WEHI3 cells expressing Ly49Q-WT showed rounded shapes and decreased adhesiveness. In contrast, WEHI3 cells expressing almost equal amounts of Ly49Q-YF adhered and spread. Control and Ly49Q-YF transfectants exhibited paxillin staining at the pericellular edges, associated with structures that looked like focal adhesions. In contrast, in the Ly49Q-WT neutrophils, paxillin staining appeared diffuse, and the focal adhesion-like structures were not distinct. Inhibition of Src kinase by Ly49Q in the steady state was consistent with this observation, because Src activity is necessary for focal adhesion formation (Parsons and Parsons, 1997). Thus, in the absence of chemoattractant, Ly49Q prevents firm adhesion in an ITIM-dependent manner. This function may be attributable to a specific feature of Ly49Q, because Ly49A did not show a comparable effect on focal adhesion formation (Figures S4A and S4B).

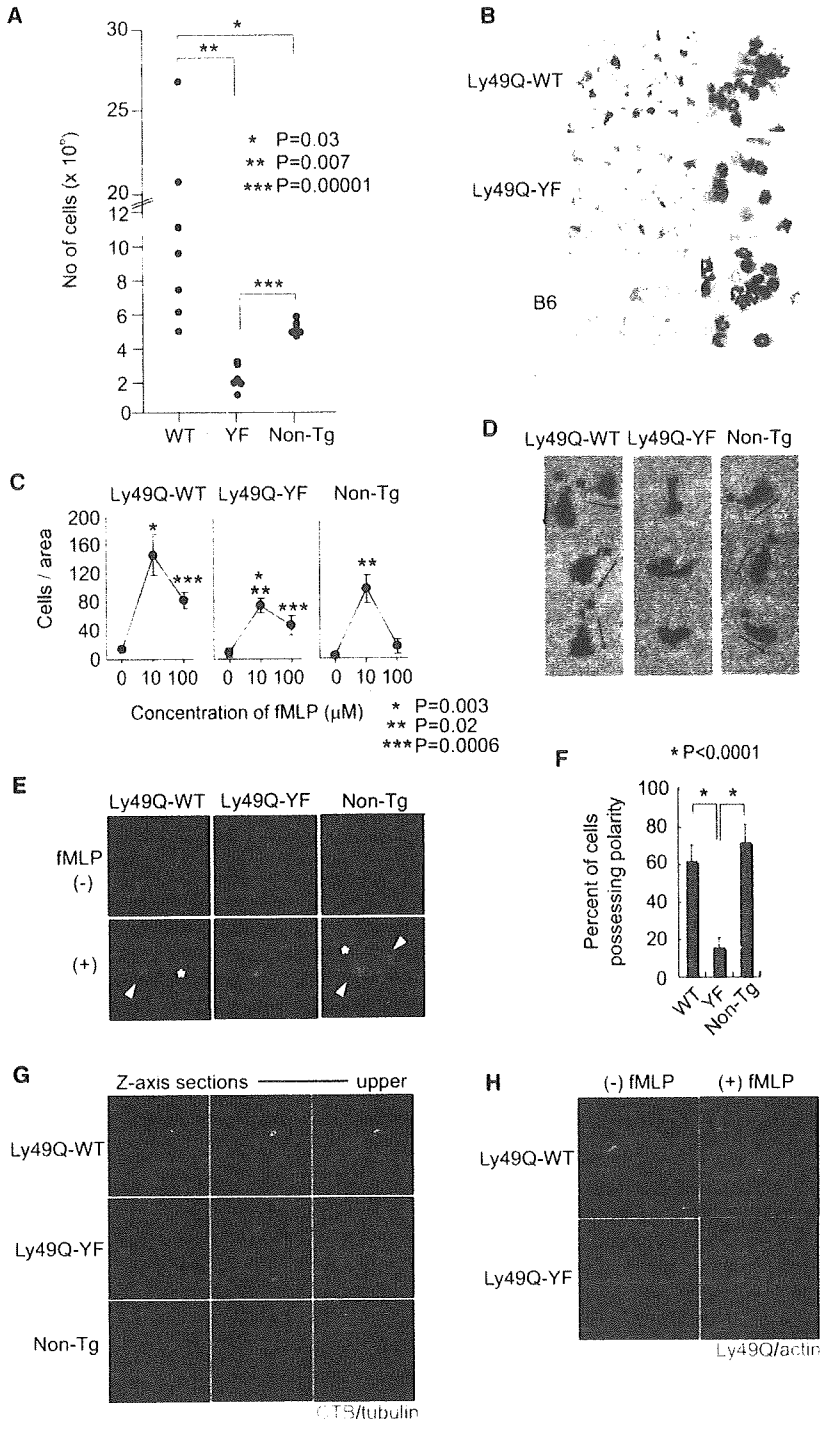

Figure 5. Impaired Neutrophil Polarization and Infiltration into Inflammatory Sites in Ly49Q-YF Tg Mice

(A) Reduced infiltration of Ly49Q-YF neutrophils into an air pouch with zymosan-induced inflammation. Three hours after zymosan injection (0.5 mg/mouse) into the air pouch, the infiltrating cells were collected and counted. The Ly49Q-WT mice were from lines 19 and 8, and the Ly49Q-YF mice were from lines 2–4 and 2–6. Three to four mice from each line were studied.

(B) The Ly49Q-YF neutrophils showed reduced invasiveness in response to fMLP. The images show transmigrated neutrophils stained with Diff-Quick.

(C) Neutrophil migration through Matrigel. At least four independent fields were photographed at 200×, and the migrated cells were counted. Data are presented as mean ± SEM.

(D) Spreading morphology of neutrophils stimulated with fMLP. Neutrophils that adhered to fibronectin-coated culture dishes in the presence of fMLP were stained with DifQuick. Arrows indicate the orientation of cellular polarity. Asterisks indicate uropodia. Neutrophils expressing Ly49Q-YF showed defective lamellipodia and filopodia formation (compare the left and right panels to the middle).

(E) Impairment of fMLP-induced polarity in Ly49Q-YF neutrophils. Confocal images show cytoskeletal organization (F-actin) stained with Alexa594-labeled phalloidin (red) in neutrophils that were polarized in response to fMLP. Arrowheads and asterisks indicate lamellipodia and uropodia, respectively.

(F) Quantitative analyses of the polarized neutrophils in response to fMLP. Neutrophils were stained with phalloidin as described in (B), the cells containing polarized actin were counted, and the percentage of polarized cells is shown. Over 100 cells from over five independent microscopic fields were counted. Results represent the mean ± SD of three separate experiments. *$p < 0.00001$. Data are presented as mean ± SEM.

(G) Impaired raft movement in Ly49Q-YF neutrophils. Neutrophils prepared from BM were incubated with fMLP and stained with CTB (green) and an anti-tubulin (red). Raft compartments were internalized and observed at the perinuclear region in the Ly49Q-WT and non-Tg neutrophils, but not in the Ly49Q-YF neutrophils. Confocal images from three planes along the z axis in the same cells are shown.

(H) ITIM-dependent redistribution of Ly49Q in response to fMLP. Confocal analysis of the intracellular distribution of Ly49Q in Tg neutrophils. Neutrophils prepared from Tg BM were incubated with or without fMLP and stained with a Ly49Q antibody (red) and phalloidin (green). The Ly49Q-WT neutrophils responded to fMLP with a marked change in Ly49Q distribution. All data are representative of three or four independent experiments.

Such functional differences between Ly49Q and Ly49A may be explained by differences in the acid resistance of their ligand-binding activity and the phosphatases they preferentially recruit (Yoshizaki et al., 2009) (Figures S4C and S4D).

Ly49Q-Dependent Raft Organization and Enhancement of the Demarcated Response of Neutrophils

Finally, we examined whether the presence of Ly49Q causes quantitative and qualitative changes in raft compartments. Using

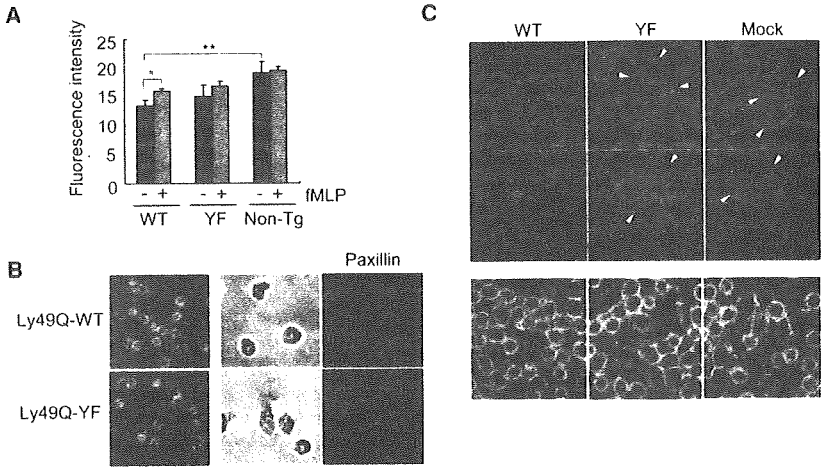

Figure 6. Effects of Ly49Q on Cell Adhesiveness and Paxillin Distribution in the Absence of fMLP

(A) Quantitative adhesion assay of BM neutrophils. Neutrophils prepared from the Tg BM were labeled with BCECF and incubated without (black bars) or with (gray bars) fMLP (25 μM) at 37°C for 40 min, and the fluorescence intensity of the lysed adherent cells was measured. Results are presented as the mean ± SD of triplicate cultures. *p = 0.04; **p = 0.007. Data are presented as mean ± SEM.

(B) Effects of the Ly49Q transgenes on neutrophil adhesion and paxillin distribution. Photographs show adherent neutrophils in the absence of fMLP. Ly49Q-YF neutrophils exhibited a spread-out morphology in the absence of fMLP. The neutrophils were stained with an anti-paxillin and Alexa594-conjugated anti-mouse IgG.

(C) Morphology and paxillin accumulation of WEHI3 cells expressing Ly49Q-YF and Ly49Q-WT. Focal adhesion complexes were labeled with the anti-paxillin (arrowheads, upper panels). Phase-contrast images of transfectants cultured on plastic dishes are shown (lower panels).

WEHI3 transfectants, the rafts were separated as detergent insoluble fractions by sucrose density-gradient centrifugation, and the distribution of raft-associated molecules, including GM1 and caveolin-1, was examined. In WEHI3 transfectants, the rafts identified by CTB binding were mainly detected in fractions 4 and 5 (Figure 7A). Interestingly, the Ly49Q-WT transfectants showed an increase in GM1 content in the detergent-insoluble fractions (Figures 7A, 7B, and 7D). A small increase in GM1 in the light fractions was also observed in the Ly49A transfectants. In addition, the amount of GM1 was increased in the intermediate-density fractions (fractions 6 to 8) of Ly49Q-WT WEHI3 compared to those of the other transfectants (Figure 7B). These intermediate-density fractions included caveolin-1 and Rab5 (Figures S5A and S5B) and were qualitatively different from the light-density fractions (fractions 3 to 5). Ly49Q itself was detectable in these intermediate fractions (Figure 7C). These results indicated that Ly49Q mediates the formation of a certain type of raft domain in an ITIM-dependent manner.

We then compared the distribution of raft-associated signaling molecules in the absence or presence of stimulation. No remarkable differences in the distribution of SHP-1 and SHP-2 were observed among the transfectants in the steady state (Figure 7E, see also Figure S5C). However, when the cells were stimulated by raft crosslinking, a noticeable redistribution of SHP-2 to the intermediate fractions was observed in Ly49Q-WT WEHI3. In contrast, in the Ly49Q-YF, mock, and Ly49A transfectants, less SHP-2 was redistributed to the intermediate fractions than in Ly49Q-WT. Surprisingly, the Src distribution was greatly influenced by the presence of Ly49Q-WT. In the absence of stimulation, there was less Src in the light and intermediate fractions of Ly49Q-WT WEHI3 than in those of the other transfectants, and it appeared to be excluded from the raft fraction (Figure 7E). On the other hand, when the cells were stimulated by raft crosslinking, a redistribution of Src to the intermediate fractions was induced in the Ly49Q-WT transfectants. In addition, phosphorylation status of the redistributed Src appeared to be changed. In contrast, in the Ly49Q-YF- and mock-transfected WEHI3, Src was constitutively broadly distributed, and the stimulation-induced redistribution and change of phosphorylation status of Src was almost undetectable. The distribution of Ly49Q-WT and Ly49Q-YF did change before and after the stimulation (data not shown). These results indicated that Ly49Q is responsible for the organization of a certain type of raft and for the correct partitioning of Src to the rafts, with the correct timing, which is important for the sharp demarcation between quiescent and active-state neutrophils.

DISCUSSION

Compared with most vertebrate cells, blood neutrophils become polarized and move quickly to immediately infiltrate inflammatory sites. To do this successfully, neutrophils possess a particular competence for polarization and directional movement (Zigmond et al., 1981). In the current study, we found, using Ly49Q-deficient mice, that an inhibitory MHC class I receptor, Ly49Q, plays a critical role in the ability of neutrophils to become polarized and infiltrate extravascular tissues. Our data demonstrated that Ly49Q was necessary for one of the key events required for adhesion and migration: the recruitment of SHP-2 and Src to the raft compartments (Lacalle et al., 2002). In parallel, Ly49Q also mediated raft internalization and redistribution, which is known to be required for cellular polarization. Our data from dominant-negative Ly49Q Tg mice and transfectants clearly demonstrated that the ITIM of Ly49Q is important for these functions. The preferential expression of Ly49Q in inflammatory cells, such as neutrophils and plasmacytoid dendritic cells, might confer on these cells the unique ability to respond immediately to inflammatory stimuli. Membrane lipid rafts play crucial roles as signaling platforms and modulate many signaling pathways in diverse biological processes, such as cell division, apoptosis, adhesion, and chemotaxis (Mañes et al., 2001; Parton

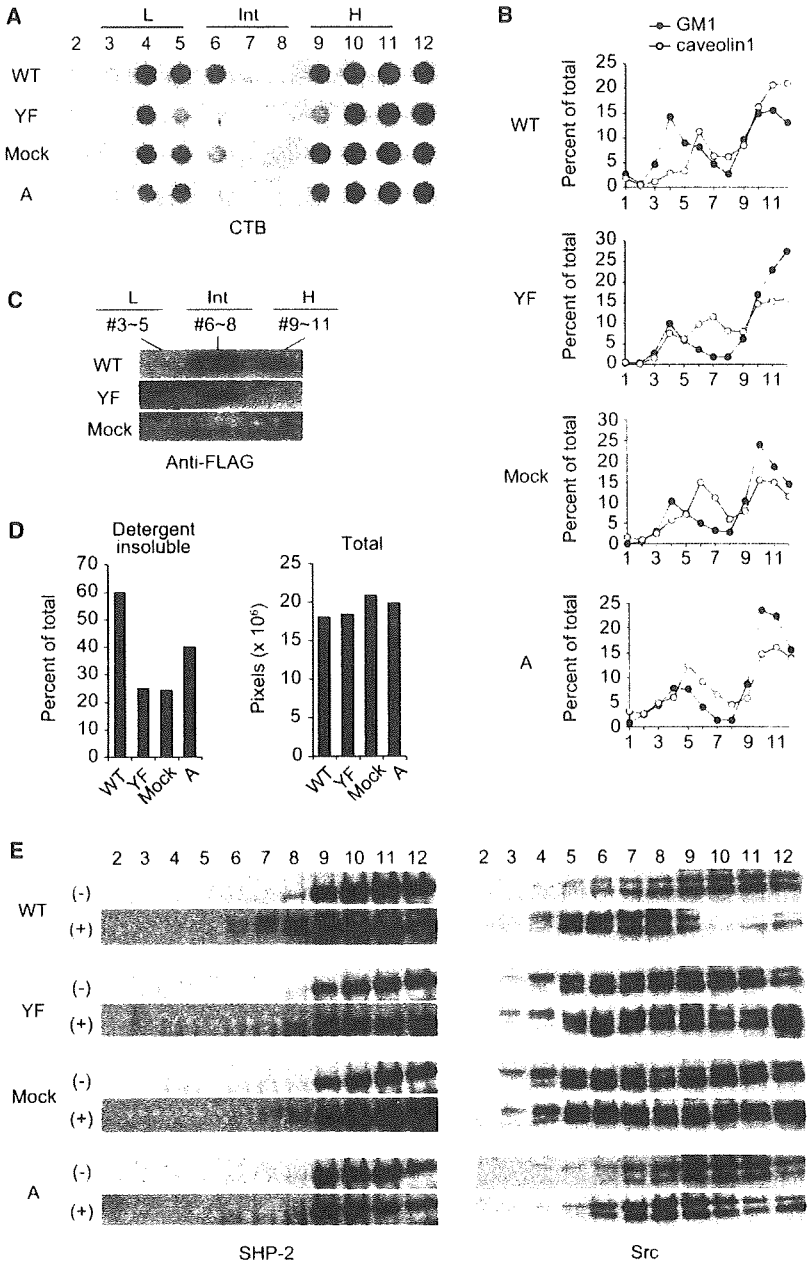

Figure 7. Effects of Ly49Q on Raft Status and Raft-Associated Signaling Molecules

(A) WEHI3 transfectants expressing Ly49Q-WT, Ly49Q-YF, mock, or Ly49A were lysed with detergent and fractionated in a sucrose gradient. Dot blotting was performed using biotin-conjugated CTB, which binds the ganglioside GM1 as a marker for of rafts.

(B) Percentage of CTB-bound GM1 and caveolin-1 in each fraction is shown.

(C) A set of three fractions from each of the low (L), intermediate (Int), and high (H) density fractions were pooled and lysed in an equal volume of 2×-concentrated RIPA buffer. FLAG-tagged Ly49Q was precipitated from the lysates and blotted with anti-FLAG.

(D) The amounts of GM1 and caveolin1 in the detergent-insoluble fractions (fractions 2–8) were determined from the pixel density and expressed as a percentage of the total pixel density in the total fractions.

(E) Cells were incubated with or without CTB (1 μg/ml) at 37°C for 30 min, and the detergent-insoluble fractions were prepared for further analysis. The fractions were separated by SDS-PAGE and subjected to immunoblotting using anti-SHP-2 and anti-Src. Experiments were performed at least in triplicate, and representative data are shown.

and Richards, 2003; Simons and Toomre, 2000). Lipid rafts also regulate the spatial targeting of the small GTPases required for cell spreading and migration (Lacalle et al., 2002). Previous studies established that lipid rafts are internalized when cells are detached from a substratum (Balasubramanian et al., 2007). The endocytosed rafts are transported in a microtubule-dependent manner to a distinct perinuclear region, where they coalesce; they are eventually returned to the plasma membrane via recycling endosomes (Balasubramanian et al., 2007). The precise mechanism underlying how Ly49Q influences raft behavior requires further investigation. The amount of GM1 in the detergent-insoluble fractions was increased in the Ly49Q-WT transfectants, but not in the Ly49Q-YF or mock transfectants, indicating that Ly49Q contributes to raft formation in an ITIM-dependent manner. This was consistent with the results of our siRNA gene targeting experiments, in which the inhibition of Ly49Q expression resulted in a decrease in CTB staining. In particular, the organization of a certain raft compartment, which was of intermediate density and included Ly49Q itself and caveolin-1, depended on Ly49Q-WT. The intermediate-density fractions appeared to be important for signal transduction, because Src and SHP-2 were recruited there when the cells underwent raft-dependent stimulation. Importantly, our data clearly indicated that Ly49Q is pivotal for the sharp demarcation between the quiescent and active states of neutrophils, which is mediated by the partitioning of Src. That is, in the steady state, Src seems to be excluded from the raft compartments by Ly49Q, but in the presence of raft-mediated stimulation, Src is recruited to certain raft compartments and phosphorylated, in a Ly49Q-dependent, ITIM-dependent manner.

Our finding that the sustained activation of Src kinase in *Klra17*$^{-/-}$ neutrophils was impaired indicated that Ly49Q is a positive regulator of fMLP-induced signals. Similarly, *Klra17*$^{-/-}$ macrophages show impaired CpG-induced activation of JNK and p38, which correlates well with the abnormal trafficking of CpG-containing endosomes (Yoshizaki et al., 2009). On the

other hand, in *Klra17*$^{+/+}$ macrophages, activated p38 and JNK are recruited to the cytosolic surface of Ly49Q-containing endosomes (Yoshizaki et al., 2009). Based on these data, it is intriguing to speculate that endocytosed rafts continue to function as a signaling platform for locally sustained signals, by maintaining the activity of the raft-associated signaling complexes. Maintenance of these activated complexes might also be beneficial for delivering them as a whole to specific regions in a cell during polarization. Although in some cases, receptor-ligand internalization has been thought to contribute to the downmodulation of a signal (Beguinot et al., 1984; Stoscheck and Carpenter, 1984), we found that the Ly49Q-MHC class I association appears to be maintained in an acidic environment (Yoshizaki et al., 2009), indicating that it at least retains the machinery required for signaling. Therefore, Ly49Q may maintain activated signaling complexes within endosomes and thereby help to transduce signals in locally partitioned regions such as the juxta-nuclear region or in the course of endosome transport along microtubules (Yoshizaki et al., 2009). We currently speculate that the intermediate-density fractions may include such signaling endosomes, because they included the endosomal marker Rab5 and Ly49Q localizes to endosomes (Yoshizaki et al., 2009).

A previous study demonstrated that the recruitment of SHP-2 to rafts is crucial for chemotactic migration via activation of the Rho small GTPase, which helps regulate the localized activation of myosin, uropodial retraction, cell-body traction, and adhesion dynamics (Lacalle et al., 2002). Therefore, the Ly49Q-dependent, stimulation-dependent partitioning of SHP-2 to the rafts may be a critical step in neutrophil migration. SHP-2 is generally a positive component of cell signaling, because this phosphatase functions upstream or downstream of various signaling molecules that activate cells, such as the EGF receptor, platelet-derived growth factor receptor, fibroblast growth factor, and Src family kinases (Poole and Jones, 2005). Recent reports also show that SHP-2 positively regulates the ERK pathway, promoting Src family kinase activation by inhibiting the recruitment of Csk to membrane fractions by dephosphorylating a Csk-targeting protein, Cbp (Dance et al., 2008; Zhang et al., 2004). Thus, the Ly49Q-mediated SHP-2 recruitment to rafts can also account for the subsequent activation of the Src and MAP kinases.

In contrast to SHP-2, SHP-1 plays a largely negative signaling role in signal transduction (Poole and Jones, 2005; Zhang et al., 2000). Negative functions of SHP-1 downstream of various immune recognition receptors, such as TCR and KIR, are well studied. Studies on moth-eaten mice have also provided strong evidence that this phosphatase plays a major role in the negative regulation of cell function (Tsui and Tsui, 1994). Our data showing Ly49Q's association with SHP-1 in the steady state suggests that Ly49Q negatively regulates cell function through SHP-1 in the absence of stimuli. This idea is supported by our finding that the tyrosine phosphorylation of Src and PI3 kinases, both of which play important roles in the positive regulation of focal adhesions formation and migration, was inhibited in the steady state by Ly49Q (Fincham et al., 2000). Therefore, Ly49Q's inhibition of focal complex formation in the steady state correlates well with its ability to inhibit the Src and PI3 kinases. PI3 kinase is a substrate for SHP-1(Poole and Jones, 2005), suggesting that SHP-1 is responsible for inhibiting the tyrosine phosphorylation of PI3 kinase.

Taken together, our data support a model in which, in the absence of chemoattractant stimuli, Ly49Q is largely located at the cell surface, where it inhibits the firm adhesion and spreading of neutrophils by preventing the stabilization of focal complexes (Webb et al., 2004). This inhibitory role includes the SHP-1-mediated inhibition of PI3 and Src kinases. When chemokine stimuli trigger the endocytosis of Ly49Q, accompanied by raft components, the process of neutrophil polarization begins. In this process, the Ly49Q ITIM and recruitment and phosphorylation of SHP-2 are crucial. These events also contribute to the sustained activation of endosomal raft-associated signaling, which accounts for the transduction of signals at compartments that are spatially and temporally segregated from the cell surface. The above model suggests a role for Ly49Q as a switching device in neutrophils. That is, it may turn off or suppress the adhesion and extravasation of neutrophils that would be deleterious in the steady state but swiftly switch on the neutrophil response to inflammation by redistributing the raft compartment to initiate polarization once a chemoattractant is encountered. Thus, Ly49Q is a dual-function receptor that functions as an inhibitory receptor in the steady state, as well as an activation receptor in the presence of inflammatory stimuli. We propose that the Ly49Q-mediated switching function from inhibitory to activating hinges on L49Q's additional recruitment of the effector phosphatase SHP-2. In addition, because Ly49Q expression is upregulated during cellular maturation (Omatsu et al., 2005), its upregulation may represent an increased potential for neutrophilic locomotion. We also speculate that the increased expression of both Ly49Q and MHC class I by IFNs (Toyama-Sorimachi et al., 2005) enhances raft functions, including phagocytosis, by increasing the raft content during inflammatory responses. Furthermore, the massive reorganization of lipid rafts resulting from the Ly49Q-MHC class I interaction would help ensure the rapid response of inflammatory cells. It is important to clarify whether human neutrophils have similar regulatory system because Ly49 family did not evolve in human. Several ITIM-bearing receptors, including ILT-LIR family members, have been identified in humans, possessing properties similar to Ly49Q regarding ligand interaction and tissue distribution (Volz et al., 2001) Therefore, a different ITIM-bearing receptor may substitute for Ly49Q function to mediate rapid response in human neutrophils.

One of the important functions of inhibitory MHC class I receptors in the context of target recognition by NK cells is to inhibit the polarization of lipid rafts and the disruption of the actin network, either of which causes the attenuation of NK cytotoxicity. In neutrophils, as we have demonstrated here, Ly49Q was integrated into lipid rafts and mediated neutrophil polarization by regulating raft status and its behavior, and the ITIM and associated phosphatases were crucial for Ly49Q's functioning. It is interesting that a similar mechanism regulates raft dynamics in immune cells ranging from myeloid cells to NK cells. Phylogenetically, given that Ly49Q is one of the oldest genes of the Ly49 family (Wilhelm et al., 2002), the Ly49 molecule may have originally functioned in lower polymorphonuclear cells, such as phagocytes, to regulate membrane dynamics through *cis* interactions with MHC class I, a mechanism that was later adopted by NK cells to recognize self MHC class I in *trans*.

In conclusion, Ly49Q functions as a switching device for the swift initiation of neutrophil polarization to produce sharply demarcated responses. Furthermore, we showed an important role for Ly49Q as a safeguard from undesirable adhesion and migration, which might be important for the maintenance of neutrophilic homeostasis. Since Ly49Q is expressed in cells that migrate rapidly to sites of inflammation and infection, Ly49Q may also act as an important device in these cells to ensure their rapid and specific responses.

EXPERIMENTAL PROCEDURES

Mice

C57BL/6J mice (6 to 7 weeks old) were purchased from CLEA Japan Inc. (Tokyo, Japan). C57BL/6 *Rag2*$^{-/-}$ mice were purchased from Taconic Farms, Inc. (Hudson, NY). Ly49Q-WT Tg mice (C57BL/6) and Ly49Q-deficient (*Klra17*$^{-/-}$) mice (129S1) were described previously (Tai et al., 2008; Yoshizaki et al., 2009). Ly49Q-deficient mice were bred with 129S1 mice, and the resulting *Klra17*$^{-/-}$ and *Klra17*$^{+/-}$ littermates were used for the same sets of experiments. Experiments for establishing Tg mice were performed according to the Guidelines for Animal Use and Experimentation set out by The Tokyo Metropolitan Institute of Medical Science (Rinshoken) (Tokyo, Japan). Experiments for analyzing Tg and Ly49Q-deficient mice were performed according to the Guidelines for Animal Use and Experimentation set out by the International Medical Center of Japan (Tokyo, Japan).

Establishment of Ly49Q-YF Tg Mice

The construction of FLAG-tagged Ly49Q-YF was described previously (Toyama-Sorimachi et al., 2004). FLAG-tagged Ly49Q-YF inserts were excised from pME18S-Ly49Q-YF with SalI and Hind III and then ligated into the Xho I sites in pCAGGS in the correct orientation. The construct for the transgene was excised from pCAGGS-Ly49Q-YF with SalI and Hind III and purified with the QIAquick Gel Extraction Kit (QIAGEN K.K., Tokyo, Japan). To screen Tg mice, genomic PCR and FACS were performed using Ly49Q-specific primers (Toyama-Sorimachi et al., 2004) and a Ly49Q antibody, respectively.

Cell Preparation

Murine neutrophils were isolated using the Histopaque-1077-Histopaque-1119 two-layer gradient method (Sigma-Aldrich, St Louis, MO) according to the manufacturer's instructions. PECs were collected by washing the peritoneal cavity with cold PBS containing 0.05% EDTA 4 hr after intraperitoneal injections of 9% casein. In the experiments of Figure 1, the neutrophils were highly purified by cell sorting with an AutoMACS (Miltenyi Biotec GmbH, Germany) using magnetic beads followed by a FACS Vantage (Becton Dickinson, San Jose, CA).

Antibodies and Reagents

Preparation of the Ly49Q antibody was described previously (Toyama-Sorimachi et al., 2004). The following mAbs were from BD Bioscience PharMingen (San Diego, CA): FITC-conjugated anti-mouse Gr-1 (RB6-8C5), PE-conjugated anti-mouse Mac-1 (M1/70), streptavidin-conjugated APC and PE, control rat IgG2a and IgG2b, anti-mouse CD18 (M18/2), and anti-CD29 (9EG7). Biotin-conjugated and purified anti-FLAG M2 were from Upstate Biotechnology Inc. (Lake Placid, NY). The anti-HA was from Roche Diagnostics GmbH (Mannheim, Germany). Antibodies against SHP-1, SHP-2, phospho-SHP-2, SHIP, Hck, Fgr, and FPR were from Santa Cruz Biotechnology Inc. (Santa Cruz, CA). Antibodies against Src and phospho-Src were from Daiichi Pure Chemicals Co. LTD. (Tokyo, Japan). TRITC-conjugated anti-paxillin was from BD Biosciences (San Jose, CA). FITC-conjugated or Alexa Fluor 594-conjugated CTB, Alexa Fluor 594-conjugated anti-rat IgG, Alexa Fluor 594-conjugated anti-mouse IgG, Alexa Fluor 488-conjugated anti-rat IgG, Alexa Fluor 633-conjugated SA, and Alexa Fluor 488- or Alexa Fluor 594-conjugated phalloidin were from Molecular Probes Inc. (Eugene, OR). PE-conjugated H-2K^{b} tetramer (T-Select H-2K^{b} OVA tetramer-SIINFEL-PE) was from Medical & Biological Laboratories Co. Ltd. (Nagoya, Japan). Zymosan A from *Saccharomyces cerevisiae* was from Sigma Aldrich (St Louis, MO). fMLP was from Sigma (St. Louis, MO) and Peptide Institute Inc. (Osaka, Japan).

Flow Cytometric Analysis

Immunofluorescence analysis was performed as previously described (Toyama-Sorimachi et al., 2004). Cytoplasmic staining was performed using the Cytofix/Cytoperm kit according to the manufacturer's instructions (BD Biosciences, San Diego, CA). Stained cells were analyzed with a FACSCalibur (Becton Dickinson, San Jose, CA).

Vectors and cDNA Transfection

WEHI3 transfectants expressing Ly49Q-WT or Ly49Q-YF were described previously (Toyama-Sorimachi et al., 2004). COS7 cells were transfected by electroporation using a Gene Pulser II (Bio-Rad Laboratories, CA). In some experiments, a Microporator MP-100 (Digital Bio, NanoEnTek Inc., Seoul, Korea) was used to introduce plasmids into RAW264.7 cells, following the manufacturer's instructions.

Immunohistochemical Staining

Cells adhering to glass coverslips or fibronectin-coated multiwell chamber slides (BD Biosciences, Bedford, MA) were fixed with 3.7% formalin in PBS at RT for 15 min, then treated with 0.1% Triton X-100 in PBS for 20 min. After being washed with PBS containing 0.05% BSA, the cells were treated with 3% BSA in PBS to prevent nonspecific protein binding. The cells were then stained with FITC-conjugated antibodies or Alexa594-labeled phalloidin. The unconjugated antibodies were visualized using Alexa488- or Alexa594-labeled second antibodies. The cells were then mounted and analyzed by confocal or fluorescence microscopy (Olympus, Hamamatsu, Japan). In the experiment using siRNA, the staining of rafts was analyzed by confocal microscopy (Zeiss, Germany) and quantified by the LC500 analysis program.

Transmigration Assay In Vitro

The in vitro transmigration assay was performed using a Chemotaxicell system with a 5 μm pore size (Kurabo Ind. LTD, Osaka, Japan). BM cells (1×10^6) in serum-free RPMI containing 2% BSA were seeded into the upper chambers of the system. In the lower chambers, fMLP at the concentrations indicated was added. After 45 min of incubation at 37°C, 5% CO_2, the cells that had migrated to the lower chamber were collected by centrifugation (1,200 rpm for 5 min at 4°C), and counted.

Neutrophil Migration Assay In Vivo

In vivo neutrophil migration was assayed using the dorsal air pouch model. Sterilized air (4 ml) was injected into the back of mice two times with a 3 day interval, followed by the injection of 1 ml of 0.5 mg/ml zymosan suspension into the air pouch. Three hours later, the cells that had infiltrated the air pouch were collected with cold PBS containing 0.05% EDTA and were counted.

Neutrophil Invasion Assay In Vitro

The neutrophil invasion assay was performed using BD Matrigel Invasion Chamber 24-well plates (8.0 μM) (BD Biosciences, Bedford, MA), according to the manufacturer's protocol with minor modification. Briefly, BM cells (2.5×10^6) in serum-free RPMI containing 2% BSA were seeded into the upper chambers of the system. In the lower chambers, fMLP at various concentrations was added. After 2.5 hr of incubation at 37°C, 5% CO_2, the filters were stained with Diff-Quick and analyzed by light microscopy (Olympus, Hamamatsu, Japan). Four randomly selected fields at 200-fold magnification were photographed, and the cells were counted. In addition, the outlines of the migrated cells were traced using ImageJ, a Java image-processing program inspired by NIH image, to determine the area in pixels occupied by the migrated cells. Outlines were drawn around cell clusters, which appeared as large islands, and around single migrated cells, which appeared as small islands. The number of pixels within the outlined areas was determined with ImageJ, and the frequencies of regions that covered more than 150 pixels were displayed as 200 pixel intervals.

Cell Adhesion Assay

The cell adhesion assay was performed as described previously with the following modifications (Toyama-Sorimachi et al., 1995). Fibronectin-coated

8-well chamber slides (BD Biosciences, Bedford, MA) were used. The adherent cells were lysed with PBS containing 1% NP-40, and the fluorescence intensity in the lysates was quantified by a Fluoroskan Ascent FC (Thermo Fisher Scientific Inc., Suwanee, GA).

Immunoprecipitation

Cells were lysed in 1% NP-40 lysis buffer consisting of 10 mM Tris-HCl (pH 7.5), 150 mM NaCl, 1 mM EGTA, 1.5 mM $MgCl_2$, 100 mM NaF, 1 mM Na_3VO_4, and complete, EDTA-free protease inhibitor mixture (Roche Diagnostics GmbH, Mannheim, Germany). The lysates were incubated with agarose beads coupled with anti-FLAG or with protein G-Sepharose coupled with the antibodies indicated. The immunoprecipitates were resolved by 5%–20% SDS-PAGE and transferred to PVDF membranes. The proteins were detected by incubating the membranes with horseradish peroxidase (HRP)-conjugated antibodies and visualized by SuperSignal West Dura Extended Duration Substrate (Pierce, Rockford, USA). In some experiments, SuperSignal West Femto Extended Duration Substrate was used for detection (Pierce, Rockford, USA). For quantification of the precipitated proteins, a LAS3000 (Fuji Photo Film Co., Ltd., Tokyo, Japan) was used.

Analysis of Tyrosine-Phosphorylated Proteins

Cells were collected in ice-cold PBS and suspended in cold 5% FCS/PBS at 1–5 × 10^6 cells/75 μl. After 25 μl of 100 μM fMLP was added, the cells were incubated at 37°C for various periods. Incubation was terminated by adding 1 ml of 1% NP-40 lysis buffer containing 100 mM NaF and 1 mM Na_3VO_4. The cell lysates were subjected to immunoprecipitation and immunoblotting.

RNA Interference

Double-stranded RNA for Ly49Q interference (UGAGGACAAUCAAGGGU CAAGAGAA) was purchased from Hokkaido System Science (Tsukuba, Japan). To introduce the siRNA into X63 cells, a myeloma cell line that expresses Ly49Q endogenously, a Microporator MP-100 (Digital Bio, NanoEnTek Inc., Seoul, Korea) was used, according to the manufacturer's instructions. Transfection efficiency was estimated by using an FITC-conjugated control siRNA-A (Santa Cruz Biotech. Inc. CA).

Sucrose-Gradient Centrifugation to Prepare Raft Compartments

WEHI3 transfectants (5 × 10^6 cells) were collected and washed with S-buffer (10 mM HEPES [pH 7.5], 150 mM NaCl, 5 mM EDTA). After cooling the cells on ice, the cells were lysed in 400 μl of Brij 96 lysis buffer (0.5% Brij 96, phosphatase inhibitors and protease inhibitors in S-buffer), and the lysates were mixed with an equal volume of 90% sucrose in S-buffer. The mixture was transferred to a centrifuge tube and sequentially overlaid with 800 μl of 35% sucrose in buffer A and 800 μl of 5% sucrose in S-buffer. After centrifugation at 55,000 rpm at 4°C for 18 hr using a Beckman optima TLX/55000), 200-μl fractions were collected from the top of the tube. For quantification of the precipitated proteins, a LAS3000 (Fuji Photo Film Co., Ltd., Tokyo, Japan) was used. The percentages of CTB-bound GM1 and caveolin-1 in each fraction (Figure 7B) were calculated as follows: % of total = pixel density in each fraction quantified by Fuji Photo Film Image Manager/sum of the pixel densities in all the fractions × 100.

Statistical Analysis

The statistical significance of differences in the values for the migration, invasion, adhesion, and spreading of neutrophils was determined with the two-tailed Student's t test. Differences with a p value less than 0.05 were considered significant.

SUPPLEMENTAL INFORMATION

The Supplemental Data include five figures and Supplemental Experimental Procedures and can be found with this article online at doi:10.1016/j.immuni.2010.01.012.

ACKNOWLEDGMENTS

We thank T. Kitamura for providing the pMxs-IRES-GFP plasmid; J. Miyazaki for the pCAGGS plasmid; M. Miyasaka, T. Sado, L.A. Miglietta, and G.E. Gray for critical reading of this manuscript; T. Okamura, S. Takahashi, and other members of JAC Inc., Japan, for animal care; and M. Ookubo, N. Sato-Yamashiro and M. Nakasuji for technical support. We also thank H. Sorimachi, K. Nishikawa, and M. Watanabe-Takahashi for helpful discussion and raft preparation and Ms. K. Furuta for secretarial support. This work was supported by grants-in-aid for Scientific Research from the Ministry of Education, Science, Sports and Culture of Japan (17590445 and 19590507 for N.T-S., 1839012 for K.I.), grants-in-aid for Research on intractable diseases from the Ministry of Health and Labour Sciences research grants (N.T.-S.), and grants from the Takeda Foundation and the Naito Foundation. S.S., M.Y., A.T., and K.F.-T. performed experiments; C.T. and H.Y. established Tg mice; T.D. helped in doing experiments; A.P.M. generated KO mice; and N.T.-S. designed the research and wrote the manuscript with K.I. and T.S.

Received: July 4, 2009
Revised: November 11, 2009
Accepted: January 22, 2010
Published online: February 11, 2010

REFERENCES

Affolter, M., and Weijer, C.J. (2005). Signaling to cytoskeletal dynamics during chemotaxis. Dev. Cell *9*, 19–34.

Balasubramanian, N., Scott, D.W., Castle, J.D., Casanova, J.E., and Schwartz, M.A. (2007). Arf6 and microtubules in adhesion-dependent trafficking of lipid rafts. Nat. Cell Biol. *9*, 1381–1391.

Beguinot, L., Lyall, R.M., Willingham, M.C., and Pastan, I. (1984). Down-regulation of the epidermal growth factor receptor in KB cells is due to receptor internalization and subsequent degradation in lysosomes. Proc. Natl. Acad. Sci. USA *81*, 2384–2388.

Ben-Neriah, Y. (2002). Regulatory functions of ubiquitination in the immune system. Nat. Immunol. *3*, 20–26.

Charest, P.G., and Firtel, R.A. (2007). Big roles for small GTPases in the control of directed cell movement. Biochem. J. *401*, 377–390.

Dance, M., Montagner, A., Salles, J.P., Yart, A., and Raynal, P. (2008). The molecular functions of Shp2 in the Ras/Mitogen-activated protein kinase (ERK1/2) pathway. Cell. Signal. *20*, 453–459.

del Pozo, M.A., Sánchez-Mateos, P., Nieto, M., and Sánchez-Madrid, F. (1995). Chemokines regulate cellular polarization and adhesion receptor redistribution during lymphocyte interaction with endothelium and extracellular matrix. Involvement of cAMP signaling pathway. J. Cell Biol. *131*, 495–508.

Downey, G.P. (1994). Mechanisms of leukocyte motility and chemotaxis. Curr. Opin. Immunol. *6*, 113–124.

Fincham, V.J., Brunton, V.G., and Frame, M.C. (2000). The SH3 domain directs acto-myosin-dependent targeting of v-Src to focal adhesions via phosphatidylinositol 3-kinase. Mol. Cell. Biol. *20*, 6518–6536.

Gómez-Moutón, C., Lacalle, R.A., Mira, E., Jiménez-Baranda, S., Barber, D.F., Carrera, A.C., Martínez-A, C., and Mañes, S. (2004). Dynamic redistribution of raft domains as an organizing platform for signaling during cell chemotaxis. J. Cell Biol. *164*, 759–768.

Grande-García, A., Echarri, A., de Rooij, J., Alderson, N.B., Waterman-Storer, C.M., Valdivielso, J.M., and del Pozo, M.A. (2007). Caveolin-1 regulates cell polarization and directional migration through Src kinase and Rho GTPases. J. Cell Biol. *177*, 683–694.

Lacalle, R.A., Mira, E., Gomez-Mouton, C., Jimenez-Baranda, S., Martinez-A, C., and Manes, S. (2002). Specific SHP-2 partitioning in raft domains triggers integrin-mediated signaling via Rho activation. J. Cell Biol. *157*, 277–289.

Lanier, L.L. (1998). NK cell receptors. Annu. Rev. Immunol. *16*, 359–393.

Makrigiannis, A.P., Pau, A.T., Schwartzberg, P.L., McVicar, D.W., Beck, T.W., and Anderson, S.K. (2002). A BAC contig map of the Ly49 gene cluster in 129 mice reveals extensive differences in gene content relative to C57BL/6 mice. Genomics *79*, 437–444.

Mañes, S., Mira, E., Gómez-Moutón, C., Lacalle, R.A., Keller, P., Labrador, J.P., and Martínez-A, C. (1999). Membrane raft microdomains mediate front-rear polarity in migrating cells. EMBO J. *18*, 6211–6220.

Mañes, S., Lacalle, R.A., Gómez-Moutón, C., del Real, G., Mira, E., and Martínez-A, C. (2001). Membrane raft microdomains in chemokine receptor function. Semin. Immunol. *13*, 147–157.

Omatsu, Y., Iyoda, T., Kimura, Y., Maki, A., Ishimori, M., Toyama-Sorimachi, N., and Inaba, K. (2005). Development of murine plasmacytoid dendritic cells defined by increased expression of an inhibitory NK receptor, Ly49Q. J. Immunol. *174*, 6657–6662.

Parsons, J.T., and Parsons, S.J. (1997). Src family protein tyrosine kinases: cooperating with growth factor and adhesion signaling pathways. Curr. Opin. Cell Biol. *9*, 187–192.

Parton, R.G., and Richards, A.A. (2003). Lipid rafts and caveolae as portals for endocytosis: new insights and common mechanisms. Traffic *4*, 724–738.

Pierini, L.M., Eddy, R.J., Fuortes, M., Seveau, S., Casulo, C., and Maxfield, F.R. (2003). Membrane lipid organization is critical for human neutrophil polarization. J. Biol. Chem. *278*, 10831–10841.

Polishchuk, R., Di Pentima, A., and Lippincott-Schwartz, J. (2004). Delivery of raft-associated, GPI-anchored proteins to the apical surface of polarized MDCK cells by a transcytotic pathway. Nat. Cell Biol. *6*, 297–307.

Poole, A.W., and Jones, M.L. (2005). A SHPing tale: perspectives on the regulation of SHP-1 and SHP-2 tyrosine phosphatases by the C-terminal tail. Cell. Signal. *17*, 1323–1332.

Ralph, P., Moore, M.A., and Nilsson, K. (1976). Lysozyme synthesis by established human and murine histiocytic lymphoma cell lines. J. Exp. Med. *143*, 1528–1533.

Scarpellino, L., Oeschger, F., Guillaume, P., Coudert, J.D., Lévy, F., Leclercq, G., and Held, W. (2007). Interactions of Ly49 family receptors with MHC class I ligands in trans and cis. J. Immunol. *178*, 1277–1284.

Servant, G., Weiner, O.D., Herzmark, P., Balla, T., Sedat, J.W., and Bourne, H.R. (2000). Polarization of chemoattractant receptor signaling during neutrophil chemotaxis. Science *287*, 1037–1040.

Simons, K., and Toomre, D. (2000). Lipid rafts and signal transduction. Nat. Rev. Mol. Cell Biol. *1*, 31–39.

Sitrin, R.G., Emery, S.L., Sassanella, T.M., Blackwood, R.A., and Petty, H.R. (2006). Selective localization of recognition complexes for leukotriene B4 and formyl-Met-Leu-Phe within lipid raft microdomains of human polymorphonuclear neutrophils. J. Immunol. *177*, 8177–8184.

Stoscheck, C.M., and Carpenter, G. (1984). Down regulation of epidermal growth factor receptors: direct demonstration of receptor degradation in human fibroblasts. J. Cell Biol. *98*, 1048–1053.

Tai, L.H., Goulet, M.L., Belanger, S., Troke, A.D., St-Laurent, A.G., Mesci, A., Toyama-Sorimachi, N., Carlyle, J.R., and Makrigiannis, A.P. (2007). Recognition of H-2K(b) by Ly49Q suggests a role for class Ia MHC regulation of plasmacytoid dendritic cell function. Mol. Immunol. *44*, 2638–2646.

Tai, L.H., Goulet, M.L., Belanger, S., Toyama-Sorimachi, N., Fodil-Cornu, N., Vidal, S.M., Troke, A.D., McVicar, D.W., and Makrigiannis, A.P. (2008). Positive regulation of plasmacytoid dendritic cell function via Ly49Q recognition of class I MHC. J. Exp. Med. *205*, 3187–3199.

Thelen, M. (2001). Dancing to the tune of chemokines. Nat. Immunol. *2*, 129–134.

Toyama-Sorimachi, N., Sorimachi, H., Tobita, Y., Kitamura, F., Yagita, H., Suzuki, K., and Miyasaka, M. (1995). A novel ligand for CD44 is serglycin, a hematopoietic cell lineage-specific proteoglycan. Possible involvement in lymphoid cell adherence and activation. J. Biol. Chem. *270*, 7437–7444.

Toyama-Sorimachi, N., Tsujimura, Y., Maruya, M., Onoda, A., Kubota, T., Koyasu, S., Inaba, K., and Karasuyama, H. (2004). Ly49Q, a member of the Ly49 family that is selectively expressed on myeloid lineage cells and involved in regulation of cytoskeletal architecture. Proc. Natl. Acad. Sci. USA *101*, 1016–1021.

Toyama-Sorimachi, N., Omatsu, Y., Onoda, A., Tsujimura, Y., Iyoda, T., Kikuchi-Maki, A., Sorimachi, H., Dohi, T., Taki, S., Inaba, K., and Karasuyama, H. (2005). Inhibitory NK receptor Ly49Q is expressed on subsets of dendritic cells in a cellular maturation- and cytokine stimulation-dependent manner. J. Immunol. *174*, 4621–4629.

Tsui, F.W., and Tsui, H.W. (1994). Molecular basis of the motheaten phenotype. Immunol. Rev. *138*, 185–206.

Volz, A., Wende, H., Laun, K., and Ziegler, A. (2001). Genesis of the ILT/LIR/MIR clusters within the human leukocyte receptor complex. Immunol. Rev. *181*, 39–51.

Webb, D.J., Donais, K., Whitmore, L.A., Thomas, S.M., Turner, C.E., Parsons, J.T., and Horwitz, A.F. (2004). FAK-Src signalling through paxillin, ERK and MLCK regulates adhesion disassembly. Nat. Cell Biol. *6*, 154–161.

Wilhelm, B.T., Gagnier, L., and Mager, D.L. (2002). Sequence analysis of the ly49 cluster in C57BL/6 mice: a rapidly evolving multigene family in the immune system. Genomics *80*, 646–661.

Wong, K., Pertz, O., Hahn, K., and Bourne, H. (2006). Neutrophil polarization: spatiotemporal dynamics of RhoA activity support a self-organizing mechanism. Proc. Natl. Acad. Sci. USA *103*, 3639–3644.

Xu, J., Wang, F., Van Keymeulen, A., Herzmark, P., Straight, A., Kelly, K., Takuwa, Y., Sugimoto, N., Mitchison, T., and Bourne, H.R. (2003). Divergent signals and cytoskeletal assemblies regulate self-organizing polarity in neutrophils. Cell *114*, 201–214.

Yoshizaki, M., Tazawa, A., Kasumi, E., Sasawatari, S., Itoh, K., Dohi, T., Sasazuki, T., Inaba, K., Makrigiannis, A.P., and Toyama-Sorimachi, N. (2009). Spatiotemporal regulation of intracellular trafficking of Toll-like receptor 9 by an inhibitory receptor, Ly49Q. Blood *114*, 1518–1527.

Zhang, J., Somani, A.K., and Siminovitch, K.A. (2000). Roles of the SHP-1 tyrosine phosphatase in the negative regulation of cell signalling. Semin. Immunol. *12*, 361–378.

Zhang, S.Q., Yang, W., Kontaridis, M.I., Bivona, T.G., Wen, G., Araki, T., Luo, J., Thompson, J.A., Schraven, B.L., Philips, M.R., and Neel, B.G. (2004). Shp2 regulates SRC family kinase activity and Ras/Erk activation by controlling Csk recruitment. Mol. Cell *13*, 341–355.

Zigmond, S.H., Levitsky, H.I., and Kreel, B.J. (1981). Cell polarity: an examination of its behavioral expression and its consequences for polymorphonuclear leukocyte chemotaxis. J. Cell Biol. *89*, 585–592.

Spatiotemporal regulation of intracellular trafficking of Toll-like receptor 9 by an inhibitory receptor, Ly49Q

*Mariko Yoshizaki,[1] *Aya Tazawa,[1] *Eiji Kasumi,[1] Shigemi Sasawatari,[1] Kenji Itoh,[2] Taeko Dohi,[1] Takehiko Sasazuki,[3] Kayo Inaba,[4] Andrew P. Makrigiannis,[5] and Noriko Toyama-Sorimachi[1]

[1]Department of Gastroenterology, Research Institute, International Medical Center of Japan, Tokyo, Japan; [2]Department of Biochemistry and Molecular Biology, Graduate School and Faculty of Medicine, University of Tokyo, Tokyo, Japan; [3]International Medical Center of Japan, Tokyo, Japan; [4]Department of Animal Development and Physiology, Graduate School of Biostudies, Kyoto University and Japan Science and Technology Agency Core Research for Engineering, Science, and Technology, Kyoto, Japan; and [5]Laboratory of Molecular Immunology, Institute de Recherches Cliniques de Montreal, Montreal, QC

Toll-like receptor (TLR) 9 recognizes unmethylated microorganismal cytosine guanine dinucleotide (CpG) DNA and elicits innate immune responses. However, the regulatory mechanisms of the TLR signaling remain elusive. We recently reported that Ly49Q, an immunoreceptor tyrosine-based inhibitory motif–bearing inhibitory receptor belonging to the natural killer receptor family, is crucial for TLR9-mediated type I interferon production by plasmacytoid dendritic cells. Ly49Q is expressed in plasmacytoid dendritic cells, macrophages, and neutrophils, but not natural killer cells. In this study, we showed that Ly49Q regulates TLR9 signaling by affecting endosome/lysosome behavior. Ly49Q colocalized with CpG in endosome/lysosome compartments. Cells lacking Ly49Q showed a disturbed redistribution of TLR9 and CpG. In particular, CpG-induced tubular endolysosomal extension was impaired in the absence of Ly49Q. Consistent with these findings, cells lacking Ly49Q showed impaired cytokine production in response to CpG-oligodeoxynucleotide. Our data highlight a novel mechanism by which TLR9 signaling is controlled through the spatiotemporal regulation of membrane trafficking by the immunoreceptor tyrosine-based inhibitory motif–bearing receptor Ly49Q. (Blood. 2009;114:1518-1527)

Introduction

Toll-like receptors (TLRs) recognize molecular patterns unique to microorganisms, and then elicit host immune responses against the pathogens. Among the TLR family members, TLR3, 4, 7, and 9 can elicit type I interferon (IFN) production in response to microbial components.[1] TLR3, 7, and 9 reside in intracellular compartments such as endosomes and detect microbial nucleic acids. The intracellular localization of such TLRs might be necessary to prevent the recognition of self nucleotides while facilitating access to microbial ones.[2] TLR9 is a sensor of unmethylated cytosine guanine dinucleotide (CpG) DNA and resides in the endoplasmic reticulum.[2,3] TLR9's recognition of CpG DNA is accompanied by changes in membrane dynamics and trafficking, resulting in a strict spatiotemporal compartmentalization of the TLR9 and CpG DNA. The CpG oligonucleotide (CpG) moves into early endosomes and is subsequently transported to a tubular endolysosomal compartment, and in both of these structures it is colocalized with TLR9.[3,4] In endosomes, TLR9 forms a complex with myeloid differentiating factor 88 (MyD88) and IFN regulatory factor 7, and activates MyD88-IFR7–dependent type I IFN induction.[5] Interestingly, the manner of CpG internalization and the retention time of CpG in endosomes differ between CpG-A and CpG-B, and the retention of CpG/TLR9 complex in the endosomes is the primary determinant of TLR9 signaling.[6] After the TLR9 signaling complexes form in endosomes, they translocate to the juxtanuclear area, in tubular endolysosomal structures that extend toward the cell periphery and plasma membrane.[3,4] However, the molecular mechanisms underlying the intracellular trafficking of TLR9 are largely unknown.

Ly49Q is an immunoreceptor tyrosine-based inhibitory motif (ITIM)–bearing inhibitory receptor belonging to the lectin-type natural killer (NK) receptor family.[7,8] However, it possesses unique distinguishing features. Ly49Q is expressed neither on NK nor NKT cells, but on plasmacytoid dendritic cells (DCs), macrophages, and neutrophils.[7,9,10] The expression of Ly49Q appears to be regulated during the maturation of these cells and is significantly up-regulated by IFN-γ treatment.[7,10,11] Ly49Q can associate with both Src homology 2-containing protein tyrosine phosphatase (SHP)-1 and SHP-2 in a tyrosine phosphorylation-dependent manner.[7] We recently reported that Ly49Q is crucial for TLR9-mediated type I IFN production by pDCs.[12] pDCs in Ly49Q-deficient mice show impaired CpG-triggered IFN-α and interleukin (IL)-12 production; consequently, TLR9-dependent antiviral responses are diminished in Ly49Q-deficient mice. To gain insight into how Ly49Q regulates TLR9 signaling, we focused on the fact that Ly49Q localizes to endosome-like vesicular compartments. We found that Ly49Q was crucial for the efficient development of the tubular endolysosomes during the intracellular trafficking of CpG and TLR9. Our results reveal a novel mechanism by which TLR signaling is controlled through the spatiotemporal regulation of membrane trafficking by the receptor Ly49Q.

Submitted December 10, 2008; accepted June 2, 2009. Prepublished online as *Blood* First Edition paper, June 15, 2009; DOI 10.1182/blood-2008-12-192344.

*M.Y., A.T., and E.K. contributed equally to this study.

This article is a continuation of a previous report.[9,12,14]

The online version of this article contains a data supplement.

The publication costs of this article were defrayed in part by page charge payment. Therefore, and solely to indicate this fact, this article is hereby marked "advertisement" in accordance with 18 USC section 1734.

Methods

Mice

Mice (6-7 weeks old) were purchased from CLEA Japan. Experiments were performed according to the Guidelines for Animal Use and Experimentation as set by the International Medical Center of Japan, and were approved by the International Medical Center of Japan. Ly49Q knockout mice were described previously.

Antibodies and reagents

The preparation of the anti-Ly49Q antibody was described previously.[7] The following monoclonal antibodies were purchased from BD Pharmingen: phycoerythrin (PE)-conjugated anti–mouse Mac-1 (M1/70); streptavidin-conjugated allophycocyanin and PE; control rat immunoglobulin (Ig)G2a and IgG2b; and anti–mouse CD18 (M18/2). Biotin-conjugated and purified anti-FLAG M2 antibodies were purchased from Upstate Biotechnology. PE-conjugated H-2K^b tetramer was purchased from MBL. Alexa Fluor 594-conjugated anti–rat IgG, Alexa Fluor 594-conjugated anti–mouse IgG, and Alexa Fluor 488-conjugated anti–rat IgG were purchased from Molecular Probes. Antibodies for phospho-c-Jun N-terminal kinase (JNK) and JNK were purchased from Santa Cruz Biotechnology. Antibodies for phospho-p38 and p38 were purchased from Dai-ichi Pure Chemicals. Antibody for Glu-tubulin was purchased from Chemicon International. Recombinant IFN-γ was purchased from PeproTech. CpG-oligodeoxynucleotide1668 and rhodamine-conjugated CpG-oligodeoxynucleotide1668 were purchased from Hokkaido System Science.

Cell culture

The murine macrophage cell line RAW264.7 was purchased from American Type Culture Collection. Cells were cultured in complete RPMI 1640 medium supplemented with 10% fetal calf serum, 10 mM HEPES (N-2-hydroxyethylpiperazine-N′-2-ethanesulfonic acid), 2 mM L-glutamine, 1 mM sodium pyruvate, 50 μM 2-mercaptoethanol, 1% (vol/vol) nonessential amino acids, 100 U/mL penicillin, and 100 μg/mL streptomycin. Macrophages and pDCs were treated with CpG-N-[1-(2,3-Dioleoyloxy)propyl]-N,N,N-trimethylammonium methylsulfate (DOTAP; Roche Diagnostics), prepared following the manufacturer's instructions. Peritoneal exudation macrophages were prepared by injecting 2 mL of 4% thioglycolate medium intraperitoneally into mice. Cells infiltrating the peritoneal cavity were collected 4 days after the injection.

Flow cytometric analysis

Acid treatment and immunofluorescence analysis were performed, as previously described.[13] Stained cells were analyzed with a FACSCalibur (BD Biosciences).

Vectors and cDNA transfection

The expression vector for TLR9-green fluorescent protein (GFP; pCAGGS-TLR9-GFP) was a gift of Dr K. Miyake (Tokyo University).[14,15] Expression vector for Rab5-DsRed was a gift of Dr C. R. Roy (Yale University). WEHI3 transfectants expressing wild-type Ly49Q (Ly49Q-WT), the ITIM-less mutant, or containing the mock vector were previously described.[7] The vectors for the Ly49Q knockdown were a gift of Dr Takayanagi (Tokyo Medical and Dental University). RAW264.7 cells were transfected by electroporation using a Microporator MP-100 (Digital Bio; NanoEnTek), following the manufacturer's instructions.

Immunohistochemical staining

Cells adhering to glass coverslips were fixed with 3.7% formalin in phosphate-buffered saline (PBS) at room temperature for 15 minutes, and then treated with 0.1% Triton X-100 in PBS for 20 minutes. After being washed with PBS containing 0.05% bovine serum albumin, the cells were treated with 3% bovine serum albumin in PBS to prevent nonspecific protein binding. The cells were then stained with the indicated antibodies or reagents, mounted, and analyzed by confocal (Zeiss) or fluorescence (Olympus) microscopy.

Western blot analyses

The cells were lysed in radioimmunoprecipitation assay buffer consisting of 10 mM Tris-HCl, pH 7.5, 150 mM NaCl, 1 mM EGTA (ethyleneglycoltetraacetic acid), 1.5 mM $MgCl_2$, 10 mM NaF, 1 mM Na_3VO_4, and complete EDTA (ethylenediaminetetraacetic acid)-free protease inhibitor mixture (Roche Diagnostics). The lysates were resolved by 5% to 20% sodium dodecyl sulfate (SDS)–polyacrylamide gel electrophoresis and transferred to polyvinylidene difluoride membranes. The proteins were detected by incubating the membranes with the indicated antibodies and visualized using SuperSignal West Dura Extended Duration Substrate (Pierce). In some experiments, SuperSignal West Femto Extended Duration Substrate was used for detection (Pierce). For quantification of the precipitated proteins, a LAS-3000 (Fuji Photo Film) was used.

Reverse transcription–polymerase chain reaction and quantification of mRNA

For RNA preparations, Isogen was used according to the manufacturer's instructions (Wako Pure Chemical). cDNA synthesis was performed according to standard protocols using oligo(dT) and random hexamer oligonucleotides. For semiquantitative reverse transcription–polymerase chain reaction (RT-PCR), gene-specific fragments were obtained by linear phase PCR amplification, and standardized using the β-actin or hypoxanthine guanine phosphoribosyl transferase 1 level. Quantitative differences in mRNA levels were determined by real-time RT-PCR using SYBR Green PCR Master Mix (Applied Biosystems) and a thermal cycler controlled by the 7900HT Fast Real Time PCR system (Applied Biosystems). Primers used for PCR analyses are shown in supplemental Table 1 (available on the *Blood* website; see the Supplemental Materials link at the top of the online article).

RNA interference

Double-stranded RNA for Ly49Q interference (UGAGGACAAUCAAGGGUCAAGAGAA) was purchased from Hokkaido System Science. To introduce the small interfering RNA (siRNA) into RAW264 cells, a Microporator MP-100 (Digital Bio; NanoEnTek) was used according to the manufacturer's instructions. Transfection efficiency was estimated by using a fluorescein isothiocyanate–conjugated control siRNA-A (Santa Cruz Biotechnology).

Statistical analysis

The statistical significance of differences in values for the migration, invasion, adhesion, and spreading of neutrophils was determined with the 2-tailed Student *t* test. Differences with a *P* value of less than .05 were considered significant.

Results

Colocalization of Ly49Q with CpG in lysosomal compartments

We recently reported that, in Ly49Q-deficient mice, the TLR9-triggered production of cytokines such as IFN-α and IL-12 is severely impaired.[12] To investigate how Ly49Q affects TLR9 signaling, we first examined whether Ly49Q colocalizes with CpG-containing endosomes. Because Ly49Q is internalized and localizes to endocytic compartments, we hypothesized that Ly49Q colocalizes with CpG/TLR9 in endosomal compartments and affects TLR9 signaling. To facilitate the immunohistochemical analyses, peritoneal macrophages expressing FLAG-tagged Ly49Q were obtained from Ly49Q-expressing transgenic (Tg) mice (supplemental Figure 1). Ly49Q was detected not only at the cell surface,

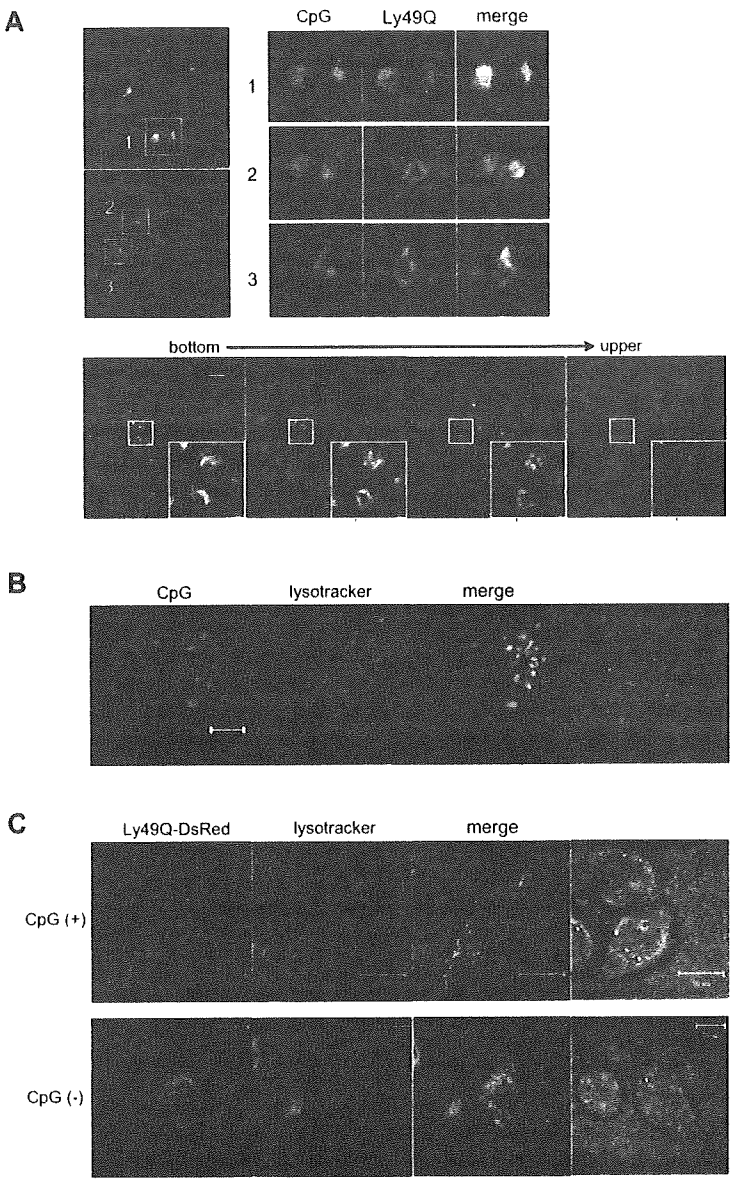

Figure 1. Ly49Q colocalized with CpG in endosome/lysosome compartments. (A) Colocalization of Ly49Q with CpG in endosomes. Peritoneal exudate macrophages were prepared from Ly49Q Tg mice. The cells were incubated with rhodamine-conjugated CpG (0.3 μM) for 15 minutes, fixed with 4% formalin in PBS, then stained with an anti-FLAG antibody and analyzed by confocal microscopy. The bottom 4 photographs show serial *Z*-axis–sectioned patterns after 60-minute incubation with rhodamine-conjugated CpG. Squares indicate the region shown in higher magnification. (B) Localization of CpG to late endosomes/lysosomes. RAW264 cells were incubated with rhodamine-conjugated CpG for 60 minutes. To visualize the late endosomes/lysosomes, the cells were incubated with lysotracker for the last 30 minutes. (C) Localization of Ly49Q in the late endosomes/lysosomes. A Ly49Q-DsRed fusion construct was introduced into RAW264 cells. Twenty-four hours after transfection, the cells were cultured with lysotracker at 37°C for 30 minutes, and the intracellular localization of Ly49Q was examined by confocal microscopy. Ly49Q localized to the late endosomes/lysosomes. In the presence of CpG stimulation, Ly49Q-containing compartments showed a tubular structure.

but also in annular-shaped vesicular compartments (Figure 1A). The CpG fluorescence partially overlapped with the Ly49Q-associated vesicles, and some of the CpG-containing endosomes were closely encircled by Ly49Q vesicular structures, suggesting that the Ly49Q-associated vesicles had fused with the CpG-containing endosomes. Z-axis sections revealed that the Ly49Q-containing compartments were intricately intertwined with the CpG-containing endosomes. Similar results were obtained using the RAW264 macrophage cell line (data not shown). As previously demonstrated, the CpG-containing endosomes subsequently acquired lysosome-like features along with acidification, which was detectable with an acidic organelle-targeting fluorescent dye (Figure 1B).[16,17] To clarify whether Ly49Q also localized to the lysosome-like compartments, a Ly49Q-DsRed fusion protein was expressed in RAW264 cells. The Ly49Q localized to lysotracker-targeted compartments in the steady state (Figure 1C). CpG stimulation caused the Ly49Q to be redistributed to tubular vesicular compartments, which were previously described as tubular endolysosomal structures.

Defective CpG redistribution and endolysosome extension in Ly49Q$^-$ pDCs and macrophages

Previous studies demonstrated that the intracellular trafficking of CpG is spatiotemporally regulated, and that the behavior of CpG endosomes affects the quality of TLR9 signaling.[5,6] Therefore, we next investigated whether Ly49Q is involved in CpG trafficking using Ly49Q$^{-/-}$ pDCs and macrophages. The internalization of CpG and its subsequent redistribution to tubular endolysosomes were observed in bone marrow-derived pDCs prepared from a Ly49Q$^{-/-}$ mouse (Figure 2A). The tubular endolysosomal structures radiated from the perinuclear region, extending toward the cell periphery. Lysosomal-associated membrane protein-1 (LAMP-1)$^+$ late endosomes were localized to the perinuclear region, and some of the CpG colocalized with LAMP-1. These results are consistent with a previous report showing that internalized CpG is transported to the perinuclear region through late endosomes and subsequently distributed into tubular endolysosomes.[3]

In contrast, Ly49Q$^{-/-}$ pDCs showed fractionated and undirected CpG-containing compartments. Only a small portion of the

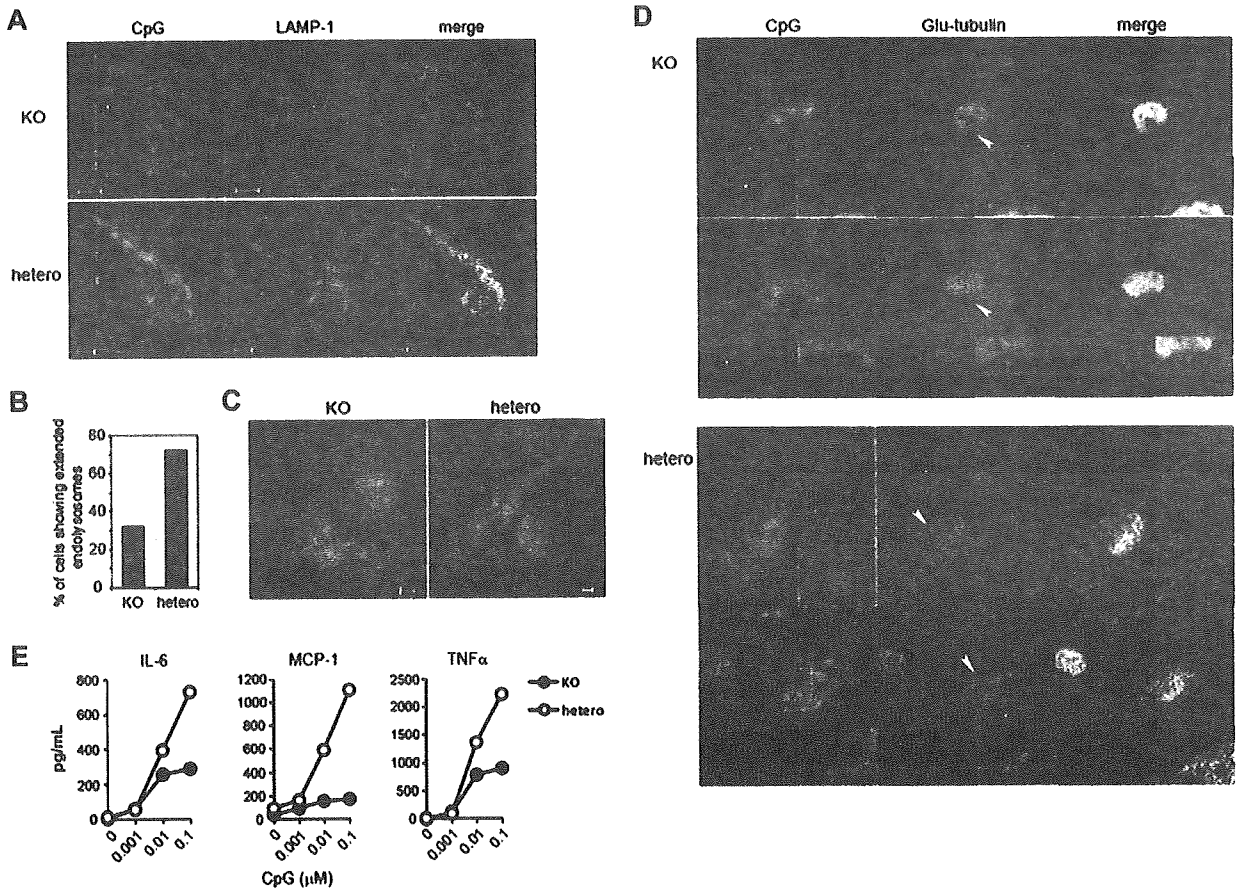

Figure 2. Formation of tubular endolysosomal structures was impaired in pDCs and macrophages derived from Ly49Q knockout mice. (A) Bone marrow–derived pDCs were prepared by culturing bone marrow cells with Flt3L, and they were then incubated with rhodamine-conjugated CpG (0.3 μM) for 60 minutes. The cells were fixed and then stained with an anti–LAMP-1 antibody. Confocal images of representative cells are shown. (B) The number of cells showing the directionally extending CpG-including tubular endolysosomal structures was counted, and the proportion of total cells was calculated. (C) Peritoneal exudate macrophages were prepared from Ly49Q knockout and control littermate mice and incubated with rhodamine-conjugated CpG (0.3 μM) for 24 hours. The intracellular distribution of CpG was examined by confocal microscopy. (D) The peritoneal exudate macrophages were treated with rhodamine-conjugated CpG (0.3 μM) for 24 hours. The cells were fixed and then stained with anti–detyrosinated tubulin (Glu-tubulin) antibody. Arrowheads indicate MTOC. (E) Cytokine production by peritoneal exudate macrophages was compared between Ly49Q-deficient and control littermate mice. Macrophages were stimulated with CpG, and the amount of cytokine in the culture supernatant was estimated by cytokine bead array 24 hours later.

CpG compartments colocalized with the late endosomes, and the perinuclear localization of the late endosomes was not obvious in the Ly49Q$^{-/-}$ pDCs. The frequency of cells possessing radiating and elongating endolysosome structures was decreased in the Ly49Q$^{-/-}$ pDCs compared with the Ly49Q$^{+/+}$ pDCs (Figure 2B). A similar defect in the redistribution of CpG-containing endolysosomes was observed in Ly49Q$^{-/-}$ peritoneal exudate macrophages (Figure 2C). The directional extension of CpG-containing endolysosomes was not observed in the Ly49Q$^{-/-}$ macrophages, whereas numerous directional CpG-containing endolysosomes elongating from the perinuclear region were observed in the Ly49Q$^{+/+}$ macrophages. The tubular endolysosome elongation has been shown to be MyD88 independent, but microtubule dependent.[3,18] Stabilized microtubules are enriched with posttranslationally modified tubulins such as detyrosinated tubulin (Glu-tubulin), in which the C-terminal tyrosine of α-tubulin is removed by tubulin carboxypeptidase.[19] Immunohistochemical staining of Glu-tubulin clearly demonstrated that, in Ly49Q$^{+/+}$ macrophages, Glu microtubules colocalized with the tubular endolysosomes, indicating that stabilized microtubules exist along the endolysosomes (Figure 2D). In addition, the Glu-tubulin at the microtubule organizing center (MTOC) appeared to be connected to the tubular endolysosomes in Ly49Q$^{+/+}$ macrophages. In contrast, in Ly49Q$^{-/-}$ macrophages, Glu-tubulin did not colocalize with the endolysosomes, and no connection between Glu-tubulin and the endosomes at the MTOC was observed. Thus, the impairment of endolysosome elongation in the Ly49Q$^{-/-}$ macrophages was associated with decreased stability of the microtubules. Consistent with these observations, in Ly49Q$^{-/-}$ macrophages, the CpG-triggered production of cytokines, including IL-6, tumor necrosis factor α, and monocyte chemoattractant protein-1, was severely diminished (Figure 2E). Thus, the absence of Ly49Q upset the CpG trafficking in both pDCs and macrophages, in close correlation with the failure of cytokine production in both pDCs and macrophages.

Importance of Ly49Q in TLR9-mediated IFN-β and IL-6 production in RAW264 cells

Next, we tried to investigate the intracellular trafficking of CpG and TLR9 in the presence or absence of Ly49Q using the mouse macrophage cell line RAW264, which expresses TLR9 and readily permits the introduction of various expression constructs. To do this, we established Ly49Q^{hi} and Ly49Q^{lo} RAW264 clones to examine the relevance of Ly49Q in CpG/TLR9 trafficking, because the expression level of Ly49Q in RAW264 cells was heterogeneous in the steady state (Figure 3A). Four clones each of Ly49Q^{hi} or

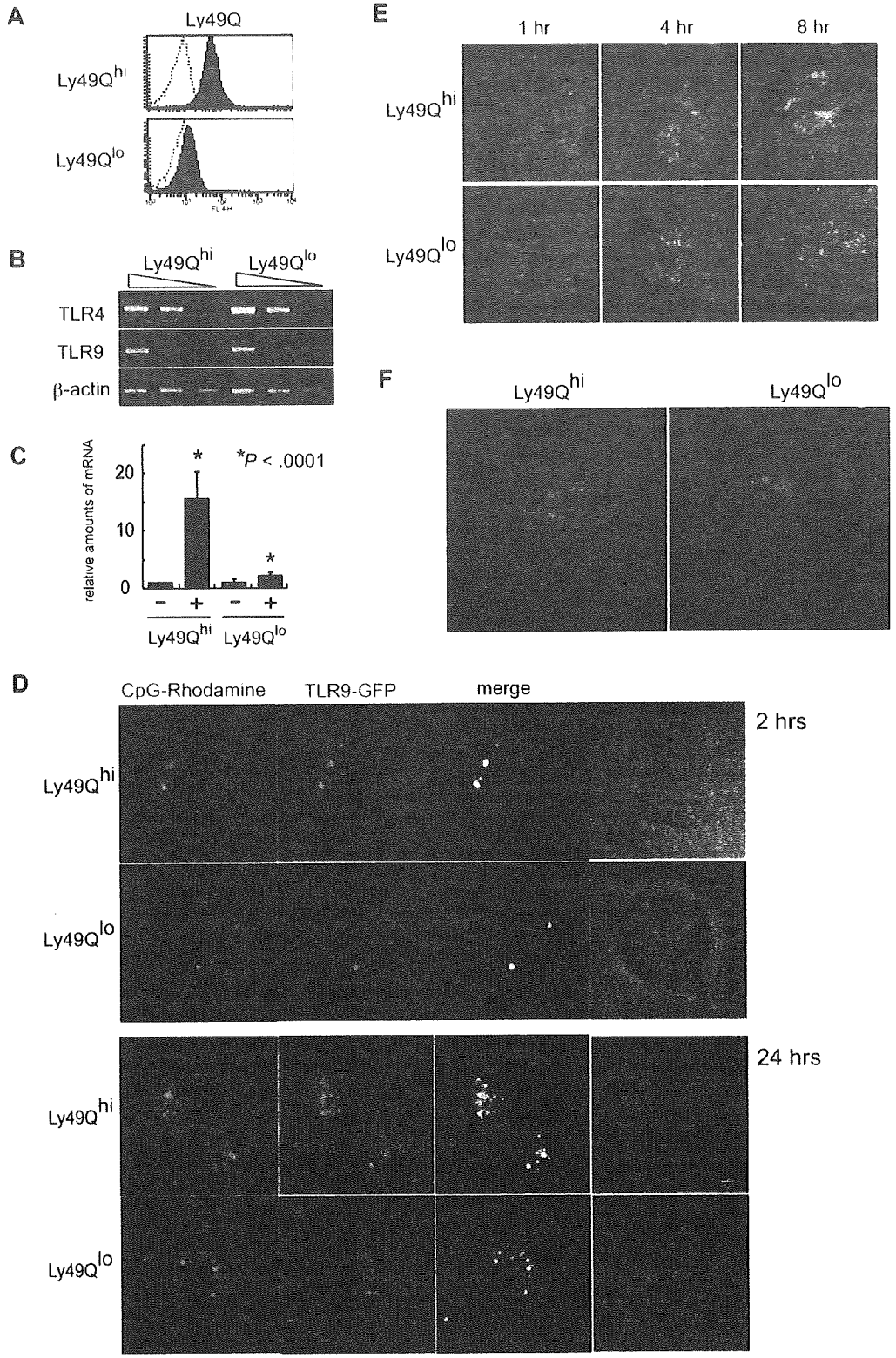

Figure 3. Inefficient uptake of CpG and retarded redistribution of TLR9 in Ly49Q^{lo} cells. (A) Expression of Ly49Q in RAW264 clones. Ly49Q^{hi} or Ly49Q^{lo} RAW264 clones were established from bulk RAW264 cells by limiting dilution. Four clones of each type were analyzed, and similar results were obtained. Data from representative clones are shown. (B) No difference in TLR9 and TLR4 expression in RAW264 cells. Semiquantitative RT-PCR was carried out using RNA prepared from the indicated cells. The presence or absence of Ly49Q had no effect on the transcription of these TLRs. In the photographs, the PCR templates were sequentially diluted by 5-fold. (C) Quantitative analysis of IFN-β transcription in RAW264 cells in response to CpG. Ly49Q^{hi} or Ly49Q^{lo} RAW264 cells were stimulated with CpG1668 (0.3 μM) for 4 hours, and quantitative RT-PCR analyses were performed. The histograms show the relative amounts of IFN-β mRNA evaluated by real-time PCR. (D) Intracellular redistribution of CpG and TLR9. TLR9-GFP expression plasmids were introduced into RAW264 cells. Twenty-four hours after transfection, the cells were incubated with rhodamine-conjugated CpG (0.3 μM) for the indicated periods. Impaired CpG/TLR9 redistribution was observed in the Ly49Q^{lo} RAW264 cells. (E) Internalization and distribution of CpG in RAW264 cells. RAW264 cells were incubated with rhodamine-conjugated CpG (0.3 μM) and fixed at the indicated time points. (F) Intracellular distribution of rhodamine-conjugated CpG. After 24 hours of incubation with CpG, tubular endolysosomal structures were observed in Ly49Q^{hi} RAW264, but not in Ly49Q^{lo} RAW264 cells.